To the Graduate Council:

I am submitting herewith a thesis written by Mary B. Groff entitled "Finite Element Thermal and Stress Analyses of Thin Cylindrical Rings of Variable Geometry Subjected to High Heat Flux Conditions." I have examined the final copy of this thesis for form and content and recommend that it be accepted in partial fulfillment of the requirements for the degree of Master of Science, with a major in Mechanical Engineering.

Roy J. Schulz

Roy J. Schulz, Major Professor

We have read this thesis
and recommend its acceptance:

Lloyd W. Crawford

James N. Chapman

Accepted for the Council:

C W Minkel

Vice Provost
and Dean of The Graduate School

FINITE ELEMENT THERMAL AND STRESS ANALYSES OF THIN CYLINDRICAL RINGS OF VARIABLE GEOMETRY SUBJECTED TO HIGH HEAT FLUX CONDITIONS

A Thesis

Presented for the

Master of Science

Degree

The University of Tennessee, Knoxville

Mary B. Groff

March 1988

ACKNOWLEDGEMENTS

The author wishes to thank her committee, Roy J. Schulz, James Chapman, and Lloyd Crawford, for their support and guidance in the preparation of this work.

In particular, the author is indebted to the staff of the Design Engineering Department; Wesley McMinn for his support and assistance in making this work possible, John Dace and Ward Johnson for their engineering experience, and Tressa Riddle for her drafting expertise.

A special thanks is due the author's husband, Russell, for his encouragement and patience during the preparation of this thesis.

ABSTRACT

The main objective of the present magnetohydrodynamic (MHD) research at The University of Tennessee Space Institute (UTSI) is to achieve long duration testing of components of the Coal Fired Flow Facility (CFFF). This requires that the water-cooled nozzle and circular aerodynamic duct of the upstream flow train be extremely durable. These upstream components are designed with a cooling-ring structure that is subject to high heat flux and pressure loadings. A thermal analysis and stress analysis of these cooling rings were performed using commercial finite element software. Two thermal loading conditions were studied; start-up and operating conditions.

The computer analysis indicated that metal surface temperatures on the plasma side of the ring were cool enough to support a solid slag layer. The rings with refractory-filled grooves developed significantly thinner slag layers. Predicted temperatures were not consistent with thermocouple measurements. High compressive stresses were predicted, indicating that plastic behavior of these rings is possible. Test results indicate that ring failures have occurred along the grooves of these rings.

TABLE OF CONTENTS

CHAPTER PAGE

LIST OF FIGURES

FIGURE PAGE

FIGURE PAGE

NOMENCLATURE

E	Modulus of Elasticity
h	Convection Coefficient
p	Pressure
q	Heat Flux
r, θ, z	Cylindrical Coordinates
T	Temperature
$\overline{T}$	Average Temperature
σ	Stress
τ	Frictional Shear Stress
μ	Coulomb friction

CHAPTER I

INTRODUCTION

The main objective of the present magnetohydrodynamic (MHD) research at the University of Tennessee Space Institute (UTSI) is to achieve long duration testing of the downstream components of the Coal Fired Flow Facility (CFFF), (Ref. 1). The CFFF was developed to demonstrate the feasibility of MHD principles for commercial power generation. This experimental facility can be divided into two divisions, generally classified as an upstream portion and a downstream portion, Figure 1.[1] The upstream components produce flow conditions (i.e. temperature, pressure, density, velocity, etc.) that would exist with an operating MHD channel present. The downstream components, beginning with the radiant furnace, Fig. 1, are typical of a conventional power plant. These components, however, are exposed to more severe operating conditions than they would see in conventional commercial operation.

The operating cycle begins with the pressurized combustor which produces a high temperature ($\sim 5000^{o}F$) ionized gas. The gas is passed through a converging-diverging nozzle accelerating it to supersonic velocities. In commercial operation, this high velocity gas would then pass through the MHD generator. Since the research contract at UTSI has as its primary concern the evaluation of the downstream components, the generator was initially replaced with an

---

[1] Figure 1 and all subsequent figures are contained in the Appendix.

"aerodynamic duct" of square cross-section, increasing in area from the nozzle to the diffuser. The persistent problem of water leaks into the flow stream from failures within this duct led to the design and installation of an aerodynamic duct of circular cross-section extending from the nozzle to the diffuser; the entire upstream flow train thus having a circular cross-section.

The previous failures in the square duct occurred after only a few hours of operation of the facility whereas after the installation of the circular duct, the components performed reliably for over 200 hours during the LMF4K test run. Components that are reliable for several hundred hours of operation under these severe conditions are required for the evaluation of the downstream components. A short term goal of the MHD program is to achieve 500 hours of continuous, reliable facility operation.

The purpose of the research done in the present study is to theoretically evaluate the performance of the nozzle and the adjoining circular diverging sections. These components are required to operate under the adverse conditions of high temperatures, high heat fluxes, and a highly erosive environment. Since the temperature of the gas stream (on the order of 5000°F) is above the melting temperatures of practical engineering materials, the combustor, nozzle, diverging sections of the aerodynamic duct, and diffuser are water cooled to maintain material temperatures below maximum operational temperatures. Also, for life cycle maximization, the thermal gradients through the walls which produce thermally induced stresses in the components, must be minimized.

The purpose of the analysis in this thesis is to better understand the performance of the mechanical design of a water-cooled, ring-type construction for the nozzle and first few aerodynamic duct sections. This thesis presents a theoretical description of the heat transfer and resulting temperatures and thermal stresses occurring within the rings. The theory is based on a finite element analysis procedure, which is outlined. The temperature distribution and associated thermal stress distribution through the walls of selected water-cooled rings in the nozzle and aerodynamic duct that are exposed to the flowing plasma stream were investigated using commercially available finite element software. A key part of the analysis is the method used to model the metallic cooling ring structures used to form the nozzle and upstream supersonic duct elements, and also, the slag coating that adheres to the exposed surfaces of the cooling rings. It is hoped that this investigation will lead to more reliable and more economical designs in the future.

CHAPTER II

NOZZLE AND CIRCULAR AERODYNAMIC DUCT

Specific components of the upstream portion of the Coal Fired Flow Facility to be studied include the nozzle and the circular aerodynamic duct, Figure 2. The circular cross-section aerodynamic duct consists of the three diverging sections, and a constant area duct that mates to a sudden-expansion diffuser.

The nozzle and diverging sections are constructed of austenitic stainless steel rings of varying inner and outer diameters, that are fitted into carbon steel shells. The constant area section consists of a cylinder within a cylinder construction and connects the diverging sections to the diffusers. The constant area section was not studied in this research.

The composite duct-section rings of the nozzle and diverging sections are all of similar construction, Figure 3.[2] A thin inner ring is welded to a thick outer ring. The inner ring is internally contoured to form water cooling passages of varying cross-section. Figure 3 shows a ring with slag grooves. Each ring assembly, consisting of the welded inner and outer rings, is 5.08 cm long. The inner surface is exposed to the flow stream. The outer ring surface is in contact with the outer steel containment shell into which it is assembled; enough tolerance is allowed for the ring to be fitted into the shell. Since the flange of the outer shell

---

[2] It will be noted that Figs. 3 through 7 are not to scale. These and all following figures having dimensions called out are in centimeters.

cylinder is trimmed flush length-wise with the ring assembly, the section acts as a unit. There is no allowance for the rings to expand within the outer shell. The nozzle, though, has a slightly different construction. There is an expansion space of approximately 0.1 cm length-wise between each inner ring. The expansion space is negligible in comparison with the amount of overall nozzle assembly expansion caused by temperature increase. Also, the minimum cross-sectional area throat ring of the nozzle has no slag grooves cut into the exposed surface in contact with the flowing plasma. The water-cooling passages are divided as shown in Fig. 4 to promote uniform cooling flow.

The rings of diverging sections #1 and #2 are of similar construction as shown in Fig. 5. Slag grooves are cut into the inside surfaces and the water-cooling passages are as shown. The rings of diverging section #3 are similar to those of sections #1 and #2, except that there are no subdividers for the flow in the water cooling passages, as shown in Fig. 6. Note that the ring shown in Fig. 6 has a variable thickness or taper. This taper results in only 20/1000 difference in the thickness of the ring. Therefore, it was neglected in the analysis. The rings analytically investigated are in diverging section #1, diverging section #3, and in the nozzle throat.

<u>Refractory</u>

The combustor of the CFFF produces simulated MHD conditions of high gas temperatures. To contain these adverse gas conditions, a refractory lining is installed on the gas side of the rings throughout the circular aerodynamic duct. The refractory is a protective coating to reduce heat transfer, and to prevent oxidation and/or diffusion of gases into the surface of the ducting. The refractory coating is required to be both physically and chemically compatible with the stainless steel. The coating does not itself supply elements for diffusion into the metal and there is minimal cracking or spalling off during thermal transient conditions. (Ref. 2)

The refractory, Jade Set Super®, consists predominantly of high purity alumina and chromic oxide. It is applied to the inner surfaces as a putty. This type of chemical composition was desired for its resistance to deterioration from the highly corrosive (reducing) plasma flow. The slag grooves are filled with refractory leaving only a negligible layer of refractory material on the surfaces of the lands or "humps". The refractory used to line the circular aerodynamic duct provides a resistance to thermal shock during pre-heat or start-up conditions and during oil and coal flow changes. The nozzle throat ring does not have a refractory coating.

The refractory lining must be accounted for in the analysis of the heat transfer characteristics of the rings. The thermal conductivity of the refractory was not available from the manufacturer. Therefore, a value was estimated based upon the chemical content of the material. The thermal conductivity of the refractory K-Jaderam®, of similar chemical composition, was available as a function of temperature, (Ref. 3). A thermal conductivity of 0.0288 W/cm K was used for the analysis in this study.

Other mechanical properties of the refractory will not be needed, as it is assumed that the refractory does not contribute to the stiffness of the ring.

Slag Coating

The UTSI MHD process is based on the combustion of coal seeded with potassium which produces a slag material that accumulates on the inner surfaces of the flow train exposed to the flowing plasma. The corrosive effects of this slag coating is combatted by the use of the refractory coating applied to the exposed surfaces. During CFFF start-up conditions, fuel oil combustion is used to establish proper conditions for coal combustion. Once coal combustion has begun, a slag layer develops along the walls forming an insulating layer. It is assumed that the surface of this layer, as it condenses out, is in a liquid phase that gradually increases in thickness and solidifies until a steady-state thickness is reached. There is then a liquid surface at or near the freezing point of the coal slag with a solid layer immediately below this extending to the refractory coating. In the case of the nozzle throat ring, the slag layer is formed directly on the metal surface of the ring since there is no refractory applied to this ring.

The chemical composition and physical properties of the coal slag need to be determined or estimated for an accurate estimate of the heat transfer through this layer. The chemical composition of the coal slag has been analyzed in previous works, (Ref. 4). Based on these chemical constituents, the thermal conductivity of the coal slag has been estimated as 0.013 W/cm K, (Ref. 5). These values indicate that the slag acts as an insulator, thus improving the operating conditions of the stainless steel cooling rings.

Loading Conditions

Conditions of high heat flux exist in the nozzle with decreasing heat flux along the length of the diverging section. The most severe conditions occur at the throat of the nozzle, which is why this ring was analyzed. The first ring of section #1 of the diverging sections was also studied, since it has different geometry and is also exposed to a high heat flux. Three thermocouples attached to this ring provided a temperature distribution for comparison to calculated values. The thermocouple placement is shown in Figure 7. All the downstream rings are of similar construction until the third diverging section is reached. The first ring of the third diverging section is exposed to a relatively lower heat flux but the cooling water passage is composed of a single large channel. Because of its differing geometry, this ring was also analyzed.

Two thermal loading conditions was applied to carry out the heat transfer and stress analyses. During start-up of the CFFF, fuel oil is burned to bring the facility to correct conditions for the combustion of coal. Without the coal slag layer covering the exposed inner rings, the rings experience a high temperature differential through the wall. However, within seconds after the coal flow has begun, a slag layer starts to build up and provides an insulating boundary on the surface of the plasma side of inner ring. The first thermal loading condition of the rings analyzed, then, was that of high heat flux during fuel oil combustion with no slag layer. The second condition was that of high heat flux during coal combustion with a steady-state slag layer during normal operating conditions.

Data for the heat flux distributions was obtained from the LMF4K test of the CFFF. The heat fluxes used for the analyses were chosen as those measured at each ring in question during the LMF4K test. The heat flux distribution is the highest during coal firing since the gas temperature increases significantly once the coal flow has begun. The oil flow distribution was chosen during the first start-up procedure during the test, during a time period of steady-state conditions. The heat flux distribution during coal flow was chosen at a steady-state period following the oil firing.

For both loading conditions, pressure loads due to the flowing plasma and cooling water were included in the analysis. The effects of the pressure loading on mechanical stresses were determined to be small compared to those caused by thermal expansion, and its contribution to the total loads is minimal; however for the sake of completeness, pressure load stress is included in the analysis.

CHAPTER III

HEAT TRANSFER

For an analysis of the stresses caused by temperature gradients, the temperature distribution through each ring must be determined. The thick outer ring was not included in this analysis since it is at the ambient temperature of the cooling water. The temperature distributions through the inner ring were investigated.

The inner ring, which is of a complicated geometry, can be idealized as a simple cylinder through which there is a radial thermal gradient. The total heat flux imposed on the rings is from the test data. The convection coefficient and mean fluid temperature in the water cooling passages are also known from experimental studies and calculation, (Ref. 6). For steady state heat conduction, with no heat generation, the temperature through the ring can be found by solving the following equation in cylindrical coordinates.

$$1/r \, [\, \partial/\partial r \, (r\partial T/\partial r)] + 1/r^2 \, (\partial^2 T/\partial \theta^2) + \partial^2 T/\partial z^2 = 0$$

This equation was derived assuming the thermal conductivity of the ring to be constant and equal in each of the three directions. The assumption was made that the conduction through the ring is axially symmetric so that the temperature is independent of θ. The assumption was also made that the ring is short with symmetric boundary conditions so that the temperature gradient with respect to z was assumed to be zero at each end of the ring.

The steady state heat conduction equation then becomes

$$1/r\ [\partial/\partial r\ (r\partial T/\partial r)] + \partial^2 T/\partial z^2 = 0$$

The boundary conditions consist of a known heat flux on the plasma side of the ring and known convection coefficient with associated mean fluid temperature in the cooling water passages. Since the inlet and outlet temperatures of the cooling water are measured during the tests, the total heat flux can then be computed. The heat transfer rate is assumed to be constant through the thickness of the ring, that is, steady-state conditions apply.

The solution of the above differential equation is straightforward by the finite element method and yields the temperature distribution through the ring. The refractory and the slag coating can also be included in the above equations by considering the ring to be a composite cylinder.

<u>Contact Resistance</u>

The temperature distribution through the rings is a function of both convection and conduction. One aspect of the conduction problem that needs to be considered is the contact resistance at the juncture of the rings, (Fig. 8). It is necessary to discuss the problem of contact resistance for completeness, although the problem will be found to be negligible for this analysis.

The contact of two metallic surfaces can have a significant influence on the heat transfer through the rings and, therefore, the temperature distribution, (Ref. 7). Reference 8 indicates that temperature distribution depends on the thermal bond between adjacent structural parts.

The heat transfer across the contact surface consists of three separate modes; the heat transfer across actual contact points, the heat transfer through a thin film of air by conduction, and the heat transfer by direct radiation. The heat transfer due to the conduction through the film of air and that due to radiation will be neglected.

The contact between two metallic surfaces is at a few discrete points. There are three factors affecting the conductance of a joint; the roughness of each surface, the flatness of the surfaces, and the way in which the surfaces fit together. As the contact pressure is increased, the peaks in contact deform and the number and size of contact points increase. The peaks of the softer surface tend to undergo plastic deformation as the harder metal's irregularities are embedded in the softer surface. The increase of pressure then tends to reduce the thermal resistance across the joint, (Ref. 7). For the rings under consideration, the high temperatures, causing large thermal expansion in the axial direction, would place the ring-to-ring interface under a large compressive pressure.

The thermal conductance of the interface also increases with mean temperature level. The compression and the temperatures would increase the thermal conductance so that the contact resistance is negligible for the ring-to-ring interfaces.

The remaining metal-to-metal interface, that of the inner ring to outer ring, will also be neglected. The water-cooling passage reduces the temperature gradient through the "legs" of the inner ring so that at the interface the thermal gradient is essentially zero and the contact resistance becomes of little importance.

CHAPTER IV

THERMAL STRESSES

Thermal Stresses Due to Temperature Difference Through the Wall

The water-cooled rings of the nozzle and diverging sections of the circular aerodynamic duct are subjected to high heat fluxes which, in turn, results in high metal temperatures. The unequal heating of the ring causes thermal gradients. The thermal gradients that exist across the thickness of the cylinder cause differential expansion from point to point. This causes internal stresses, (Ref. 9). If the stresses of the rings are assumed to be elastic, the stresses due to thermal gradients can be superimposed on the stresses caused by external loads, such as internal pressure due to the cooling water.

Thermal Stresses Due to Ambient Versus Operating Conditions

During the start-up of the facility, the temperature of the rings increases from the ambient temperature to that of operating conditions, a matter of several hundred degrees Fahrenheit. The inner rings are then exposed to an overall temperature differential causing the ring to expand both radially and longitudinally. Since the rings in the aerodynamic duct have no allowance for expansion and those in the nozzle have only a minimal allowance, stresses are induced by this suppression of elongation.

The combination of these thermally induced stresses indicates that extremely large stresses within the rings can be expected. A discussion of possible failure mechanisms is therefore included.

Thermal Stress Fatigue

Stainless steels are used for components operating at adverse conditions such as these since they exhibit good resistance to corrosion and oxidation as well as high strengths at elevated temperatures. But consistent high-temperature operating conditions can affect the material adversely. The stainless steel of the rings is a ductile material and can normally withstand additional strains, (Ref. 9). Surface failure can occur as a result of shear stress induced by compression; however, the failure process in ductile materials is progressive with the dominating factor being the metallurgy of the material. Once plastic flow begins, metallurgical changes occur. It has been found experimentally that in some cases plastic flow tends to improve the material, (Ref. 9). The material would then undergo a permanent change in shape without fracture since fracture rarely occurs in ductile materials under compression.

Thermal stress fatigue would be a possible mode of failure, being directly related to the number of start-up cycles to which the rings are exposed. Large plastic strains can be related to low-cycle fatigue. In this analysis, where temperature changes are severe and fairly rapid between start-up, operating, and shutdown conditions, thermal fatigue could be an important failure mechanism. Thermal fatigue can not be prevented by altering environmental conditions or by protective coatings. Only the elimination of the thermal cycling will prevent the thermal fatigue, (Ref. 10).

Buckling

Another mode of failure experienced by ductile materials under compressive loading is buckling. The evaluation of buckling resistance involves the consideration of certain factors. A few of these factors are the uncertainty of boundary conditions and inelastic effects on the material properties, such as strain-hardening. An accurate prediction of a cylinder's compressive strength is not always possible, (Ref. 11). Due to the uncertainty of the failure criterion in compression, the yield stress in compression is assumed to be equal to the yield stress in tension, although the compressive yield stress is usually different from, and somewhat greater than, that in tension. Plastic buckling may occur at loads for which any part of the material is stressed beyond its proportional limit, (Ref. 12).

Another factor in the evaluation of buckling resistance is the effect of the edges in short cylinders. If radial movement is allowed at the ends, the cylinder will retain its cylindrical shape thus reducing the possibility of buckling, (Ref. 13). The friction between adjoining cylinders, then, becomes important.

If the cylinders each expand due to the thermal gradients at the same rate, the ends of the rings would not experience any friction. But since the heat flux varies along the channel, it is possible that each ring assembly could be expanding both radially and axially at different rates. Friction forces can never be completely eliminated. These forces can increase the apparent resistance to compression. The shorter the cylinder, the higher the resistance to deformation. The sliding resistance between the adjoining rings is known as Coulomb friction. The drag opposing the lateral displacement of material, $\mu\sigma$, is actually a shear stress, τ. This frictional shear stress cannot exceed the yield strength in shear. Whenever the product of μ and the normal pressure exceeds this value, Coulomb friction is replaced by plastic shear in the layer of metal closest to the contact boundary. This causes the rings to "stick" rather than slide along their interface, (Ref. 14). Since the coefficient of friction can be large on high temperature surfaces, the conditions existing between the rings would be that of little sliding and predominantly sticking. Sticking reduces the maximum normal stress. A cylinder compressed with high friction conditions would have a tendency to become work-hardened, (Ref. 14). The work-hardening produces an increase in stress which allows for further plastic deformation. Thus, it is possible for the rings to undergo a plastic deformation due to the high temperature and compressive loads and, when cooled, to become work-hardened.

CHAPTER V

FINITE ELEMENT MODELLING

Finite Element Methodology

The thermal analysis and thermal stress analysis were performed using a commercial finite element program called GIFTS distributed by CASA/GIFTS, Inc. A brief discussion of the finite element method is presented here to provide an understanding of the methodology used in the evaluation of the resultant stresses and temperatures in the cooling rings.

The behavior of complex physical systems is simulated by mathematical models formulated from the theories of continuum mechanics. These physical systems are usually described in terms of partial differential equations. The finite element method is a numerical method of solving a discretized algebraic equation or set of equations that replace the given partial differential equations and their given boundary conditions. Numerical algorithms are used to solve the resulting system of algebraic equations. The numerical solutions almost always require computer implementation, (Ref. 15).

The physical systems under consideration can be represented by a continuous system, a set of partial differential equations with specified boundary conditions, (Ref. 16).

Two physical systems are considered; heat conduction through a solid and the theory of elasticity of a solid. Appropriate boundary conditions are applied to the systems. The finite element method approximates these continuous functions by a set of algebraic equations. Numerical methods are used to solve the resultant set of equations. The solution of the system of equations yields temperatures, in the case of heat transfer analysis, or displacements, in the case of elasticity or stress analysis. Once the nodal displacements (or temperatures) are known, the element strains and stresses (thermal gradients in the case of heat conduction) can be calulated.

Implementation of the Finite Element Method

The implementation of the finite element method can generally be divided into four phases; model generation, application of boundary and loading conditions, solution of the system of equations, and display of the results.

The first phase involves the discretization of the physical continuum. The approximation of a physical continuum by a finite number of elements is the first and most important step in the accurate analysis of the given problem. This step places much emphasis on engineering judgement. The type and size of element must be determined based upon the continuum under consideration.

The type of element chosen depends upon the problem and the types of elements existing on the user's software. Typical elements include three-dimensional "brick" elements, two-dimensional triangular or quadrilateral elements, and one-dimensional line elements. Models could consist of a single type of element or a combination of the previously listed elements. In many cases, the large number of unknowns involved in the use of brick elements make their use impractical when the available computer memory is limited. The size of the elements is a balance between desired accuracy, computer capabilities, and cost. The finer the mesh, the better the model can resolve regions of high gradients of properties, temperatures, and stresses. Cost and computer memory limitations limit the number of unknowns or degrees of freedom possible for the model.

Boundary conditions for the thermal and stress analysis are applied to the discretized domain. The boundary conditions can be applied at a point, along a line, or over a surface. A model being analyzed for heat transfer might have boundary conditions of constant or varying heat flux, temperature, or convective heat transfer. Stress analysis requires fixing the domain in space by applying restrictions on the degrees of freedom for nodes, lines, and/or surfaces with forces, moments, or displacements applied.

The analysis of the model proceeds then by the assembly of element stiffness (or conductance, in the case of heat transfer) matrices. The individual element stiffness matrices are assembled to form the global stiffness matrix. The solution of the system of equations is performed, yielding the temperatures for heat transfer analysis or displacements for stress analysis.

The final phase is the display of the results. From the nodal temperatures, temperature gradients are determined. From the nodal displacements, elements strains, or stresses, are calculated. Graphical displays of resultant values are valuable for the evaluation of the results. The validity of the results are examined based upon initial estimates of the model's behavior, and experimental data, where available. Inconsistent or physically implausible results require that the analyst review the assumed model geometry as well as the boundary and loading conditions. Accurate results depend upon the good engineering judgement of the user, and are often obtained by trial and error improvements in the model.

CHAPTER VI

COMPUTER MODEL

Model Generation

The thermal and stress analyses of the inner rings were performed using the GIFTS software package distributed by CASA/GIFTS Inc. The cylindrical geometry of the rings lends itself to the use of axisymmetric elements. At the time of this analysis, however, these elements are not available on the UTSI version of the software. Therefore, a thin slice (arbitrarily chosen as 0.1 cm) was taken through the cross-section of each ring and modelled as a 2-dimensional domain. The elements were chosen to be first order quadrilateral membrane elements, and only stresses in the plane of the cross-section were determined. The above choice of element was based upon computer-time considerations as well as computer memory limitations. The longitudinal symmetry of the ring cross-section allowed the modelling of only half of the ring. The circular nature of the water-cooling passages and the necessity of adding a thin layer representing the coal slag layer dictated the size of the elements. Each of the three ring sections analyzed involved two models; one without a slag layer, i.e. start-up conditions, and one with a slag layer, i.e. operating conditions. These models are shown in Figures 9 through 14.

Coal combustion leads to the formation of a coal slag layer on the surfaces of the nozzle and aerodynamic duct. An estimate of the thickness of the slag layer was made based on the thickness of the solid layer present after the completion of a test run, however, the actual determination of the thickness of the coal slag layer for the model is an iterative process. A thickness is chosen, thermal boundary conditions applied, and a thermal analysis completed. The slag layer thickness is modified until the solution predicts a slag surface temperature of approximately 1250°C, the freezing point of the coal slag. This slag thickness is then considered the equilibrium, steady-state slag thickness during coal-burning operating conditions.

Thermal Boundary Conditions

A heat flux is applied to the plasma side of the ring while convective heat transfer conditions exist along the water-cooling passages. Heat flux values were determined from experimental data from test LMF4K for each ring. Measured heat fluxes for the rings being analyzed are listed as follows for both oil and coal flows.

Location	Heat Fluxes (W/cm^2)	
	Oil Flow	Coal Flow
Throat Ring	160	180
Ring #1	160	180
Ring #31	75	120

An average water temperature of 37.8°C was assumed based on test data from the CFFF, as well as a constant convective heat transfer coefficient. Since the variation of measured water temperatures in the cooling water circuit is less that 15 per cent, the average water temperature used is within reasonable limits. The remaining sides of the ring were treated as insulated to simulate the $\partial/\partial z = 0$ condition; basically, the heat transfer between rings was considered negligible. The bottom edges of the "legs" of the rings in contact with the outer ring were also considered to be insulated since they are nearly at ambient conditions. Those surfaces where the thermal gradient was assumed to be negligible are noted on the figures displaying thermal boundary conditions.

Boundary and Loading Conditions

The stress analysis of the rings required the application of boundary and loading conditions. The rings were assumed fixed at the outer edges of the base in contact with the outer ring (at the location of the weld) but were allowed to grow in the y-direction only, along any radius of the ring. The ability of the rings to grow in the x-direction (along the centerline of the duct) was considered negligible. Symmetry conditions were applied at the right edge of the model since only the left half of the model was analyzed. Pressure loads of 24.13 N/cm^2 and 103.4 N/cm^2 were distributed along the plasma side and water side, respectively, which correspond to test conditions.

Material Properties

The inner ring is made of 347 stainless steel, whose material properties are listed in Table 1. The refractory and the slag layer were included in the analysis only from a thermal conduction aspect. Neither the refractory nor the slag coating add any stiffness to the rings and therefore the only material property necessary for the overall analysis was the thermal conductivity. The coefficient of thermal expansion used for the refractory was also assumed for the slag layer. These values are noted in Table 1.

Table 1. Material Properties Used for the Finite Element Analysis

Material	E (N/cm^2)	Thermal Conductivity ($W/cm\ ^oC$)	Coefficient of Thermal Expansion ($cm/cm/^oC$)
347 SS	1.93E07	0.1723	16.76E-06
Refractory	1	0.0288	1.0E-06
Coal Slag	1	0.013	1.0E-06

CHAPTER VII

RESULTS

The results of the thermal and stress analyses are presented in this chapter without explanation. The discussion of the results is found in Chapter VIII. For each loading case considered there will be included computer generated plots of (1) thermal boundary conditions (with units as shown), (2) temperature distributions through the ring (in units of ^{o}C), (3) pressure loads and constraints (in units as shown), (4) deflected shapes of the rings (with the undeflected model shown with a dashed line), and (5) maximum principal stresses (in N/cm^2). The thermal loading condition of heat flux along a line is designated on the computer plots as circles whose diameters are dependent upon the element size. Pressure loads are likewise depicted as arrows on the plots with the arrow size related to the magnitude of the load and the element size.

Nozzle Throat Ring Model

Oil Flow Conditions

The thermal boundary conditions applied to the model are shown in Figure 15. A heat flux of 160 W/cm^2 was applied to the plasma side of the ring. The thermal analysis yielded a temperature distribution through the ring and a plot of selected isotherms is presented in Fig. 16.

The stress analysis boundary and loading conditions applied are shown in Figure 17. The temperature distribution is internally converted into nodal thermal loads and a thermal stress analysis is then performed by the program. The resulting deflected shape of the ring is shown in Fig. 18. The maximum principal stress distribution is plotted in Fig. 19.

Coal Flow Conditions

A heat flux of 180 W/cm^2 was applied to the plasma side of the ring, Fig. 20. A thermal analysis was performed from which a temperature distribution was plotted, Fig. 21. The surface of the coal slag layer is at approximately the freezing point of the liquid slag material indicating that the thickness assumed, 0.1 cm, is a reasonable estimate for the equilibrium slag thickness for this ring.

For the stress analysis, since the slag layer has no stiffness associated with it, the modulus of elasticity in the elements modelling the slag was set equal to one. The same boundary and loading conditions were applied as for the oil flow case. Pressure loads were distributed along the plasma and water-side boundaries. Figure 22 shows the pressure loads and restraints placed upon the model. The computer stress analysis was then performed. A graphical display of the unloaded and the deflected shape can be viewed in Fig. 23 while a plot of maximum principal stresses is presented in Fig. 24.

Ring #1 model

Oil Flow Conditions

The computer model of ring #1 included the slag grooves and refractory coating of the actual hardware. A heat flux of 160 W/cm^2 was used on the plasma side of the ring, Fig. 25. Thermal analysis yielded a temperature distribution from which a plot of selected isotherms is presented in Fig. 26.

Nodal temperatures were used to compute thermal loads. Pressure loads and boundary restraints for this ring are shown in Fig. 27. A modulus of elasticity for the refractory was chosen to be one as for the coal slag. The stress analysis yielded deflections and principal stresses, Figs. 28 and 29.

Coal Flow Conditions

A coal slag layer thickness was chosen, thermal boundary conditions applied with a heat flux of 180 W/cm^2, Fig. 30, and a thermal analysis completed. The thickness was modified until the surface temperature was at the freezing point of the coal slag. Figure 31 is a plot of isotherms for an acceptable slag thickness, which was determined to be 0.02 cm.

Pressure loads and boundary restraints applied are shown in Fig. 32. Solution of the system of equations yielded the deflections and stresses shown in Fig. 33 and Fig. 34, respectively.

Ring #31 Model

Oil Flow Conditions

The model of ring #31 included slag grooves and a single, large water-cooling passage. A heat flux of 75 W/cm^2 was distributed along the plasma side of the ring, Fig. 35. Temperature profiles are plotted in Fig. 36.

Pressure loads are shown in Fig. 37, as well as restraints on the model. The previous procedure was followed to obtain the results of the deflections and principal stresses in Figs. 38 and 39.

Coal Flow Conditions

The thickness of the coal slag layer was determined in the same manner as described for ring #1 and was found to be 0.06 cm. Thermal boundary conditions, with a heat flux of 120 W/cm^2, are shown in Fig. 40 with the resultant temperature distribution in Fig. 41. Stress analysis boundary conditions are displayed in Fig. 42. Resultant deflections and principal stresses are presented in Figs. 43 and 44, respectively.

Summary of Results

Selected values of the previous results are summarized in Table 2. Maximum temperatures and compressive principal stresses are listed for each loading condition. Slag layer thicknesses are also tabulated.

Table 2. Summary of Results

	Slag Thickness (cm)	Max. Metal Temperature (^{o}C)	Max. Compressive Stresses (N/cm^2)
Throat Ring (Oil)		550	160,000
Throat Ring (Coal)	0.1	200	45,000
Ring #1 (Oil)		900(400)[a]	120,000
Ring #1 (Coal)	0.02	1000(450)	150,000
Ring #31 (Oil)		400(200)	60,000
Ring #31 (Coal)	0.06	700(300)	120,000

[a] Temperatures in parentheses are those predicted at the bottom of the groove.

CHAPTER VIII

DISCUSSION OF THE RESULTS

Accuracy of the Computer Model

The approximation of the behavior of a cylinder by a two-dimensional model of a slice through its cross-section leads to modelling inaccuracies. A cylinder in compression behaves in a different manner than a thin plate compressed on its thin sides. A cylinder in compression would resist compressive stresses better than a flat plate.

The size of the elements in the computer model are important in the evaluation of resultant values. In this case, the element size could not be decreased further without reaching the memory limitations of the personal computer being utilized. Since no stress concentrations are seen at the corners of the grooves, the element must be too large to exhibit this phenomena. Also, sharp changes in stress contour lines indicate that the element size is not small enough to display the continuous changes in stress levels.

A square element with equal adjacent sides is the best geometric form for the approximation polynomial, (Ref. 17). During the iterative process of determining the thickness of the coal slag layer of ring #1, the elements in this area are reduced only along one dimension. This leads to a long, thin element that could introduce errors in either the thermal analysis or stress analysis of this particular ring.

Solid Slag Development

All of the models, with or without the coal slag layer, exhibit high temperatures along the plasma metal surface. The temperatures, though, remained below the freezing point of the coal slag indicating that a solid layer of slag does exist along the plasma-side surface of the rings. A slag thickness of 0.1 cm is calculated for the throat ring, whereas the next ring downstream, ring #1, has a slag coating of 0.02 cm, a significant reduction, perhaps due to better cooling in the throat ring. The coating has increased to 0.06 cm at ring #31, although substantially less than that of the throat ring. This seems to indicate that the grooves in the rings tend to inhibit rather than encourage slag coating development. Temperatures of the coal slag above the refractory are greater than the melting point of the slag. These areas must either have a liquid, flowing slag thickness present or the refractory must deteriorate in thickness by erosion sufficiently to leave a cooler surface to support a solid slag layer. Thus, the model predicts that the surface of the refractory-grooved ring will become wavey on the plasma side.

Discussion of Temperature Profiles

The temperature profiles are flat or one-dimensional in the interior of the rings, becoming wavy or two-dimensional near the water-cooling passages and the plasma side with refractory grooves. Overall, the profiles become more uniform with the presence of the coal slag layer. Since the refractory and the slag coating have high thermal resistivity, large temperature gradients are evident in these areas.

Metal surface temperatures of the nozzle throat ring drop from nearly 500^{o}C during oil combustion to 200^{o}C during coal combustion, although the surface of the slag is at nearly 1200^{o}C. This drop in maximum metal temperature does not appear in the models of rings #1 and #31 for the transition from oil to coal. The insulating effects of the slag are particularly evident in the throat ring.

The slag layer thickness for ring #1 provides a minimal insulating boundary so that metal temperatures of the ring remain essentially constant for oil and coal flows, despite the increase in heat flux during coal flow. Metal temperatures on the lands average from 850^{o}C during oil flow to about 950^{o}C during coal flow, showing a slight increase in metal temperatures. The increase of metal temperature becomes less as the distance from the plasma surface increases. The slag layer, then, nearly compensates for the 20 W/cm^2 increase in heat flux.

Ring #31 has a pronounced increase of predicted metal temperatures with the combustion of coal. This ring, though, experiences more than twice the increase of heat flux, 45 W/cm^2, as that of the throat ring or ring #1. The slag layer provides some insulation but not enough to decrease the metal temperatures or keep the temperatures constant. Maximum metal temperatures on the lands average 400^{o}C during oil flow to 650^{o}C during coal flow.

Comparison of Computed Temperatures with Experimental Values

Since thermocouple measurements are available at ring #1, a comparison was made between predicted and measured metal temperatures. The temperatures measured during oil flow are plotted in Fig. 45. The average temperature of thermocouple T1 during oil flow is approximately 315°C (600°F) which is significantly lower than the predicted value of 500°C (Figure 26). It will be noted that the predicted value used is located at the bottom of the groove, which is close to the actual location of the thermocouple. At the position of thermocouple T2, a measured value of 135°C (275°F) is compared with a predicted value of 250°C. Thermocouple T3, with an average value of 60°C (140°F), compares with 120°C predicted temperature.

There is a larger and more apparent conflict in temperatures during coal flow. Temperature measurements indicate a significant drop in temperatures immediately upon the introduction of coal combustion, Fig. 45. Thermocouple measurements during coal flow are 148°C (300°F) at thermocouple T1, 121°C (250°F) at thermocouple T2, and 60°C (140°F) at thermocouple T3. Figure 31, though, indicates that the finite element analysis predicts temperatures at thermocouple locations T1, T2, and T3 of 600°C, 280°C, and 150°C, respectively. The previous comparison is summarized in Table 3.

Table 3. Comparison of Computed Temperatures with Experimental Values

Thermocouple Location	Oil Flow		Coal Flow	
	Predicted Temp (^{o}C)	Actual Temp(^{o}C)	Predicted Temp (^{o}C)	Actual Temp (^{o}C)
T1	500	315	600	148
T2	250	135	280	121
T3	120	60	150	60

The throat ring and ring #1 are exposed to approximately the same heat flux, respectively, during each of the two conditions. The throat ring, which has no slag grooves, exhibits the behavior indicated by the thermocouple measurements. The finite element model of ring #1 during oil flow produces much higher temperatures than those measured. The predicted temperatures are nearly twice those obtained through experimental methods. Once the coal slag layer forms during operating conditions of coal combustion, the calculated temperatures of the throat ring drop, as indicated by the thermocouples, whereas the calculated temperatures of ring #1 increase with a slag layer present. This seems to indicate that the finite element model of ring #1 may not correctly imitate the real life situation as accurately as the throat ring model. Once coal combustion begins, the refractory coating within the grooves may deteriorate leaving a thin slag layer within each groove. The presence of a flowing liquid slag layer has been neglected and at this point its importance may become significant. The liquid slag may provide an appreciable insulating thickness, thus reducing the temperature gradient through the ring and reducing metal temperatures.

The theoretical predictions are consistent in that a greater heat flux during coal combustion must produce higher temperatuers in the model for constant thermal conductivities and water-side convective heat transfer. The experimental measurements, however, are not consistent with the increase in heat flux measurements obtained from the cooling-water circuits.

Discussion of Stress Contours

High compressive stresses are predicted in all of the ring models. Maximum principal stresses in the throat ring are reduced drastically from 160,000 N/cm^2 to 45,000 N/cm^2 once coal combustion begins. The oil flow stresses exist during the initial start-up, and any time the coal flow stops. However, oil-coal transition cycles would not subject the throat ring to larger principal stresses.

Sharp peaks in the stress contour line representing zero stress are possibly due to the element size. A fine mesh might display a smooth transition. It is also noted that the stress contours continue into the refractory and slag coating. The inability to delete the refractory and slag layer elements during the stress analysis leads to the assigning of a small, arbitrary modulus of elasticity, implying a negligible stiffness, as previously assumed. The element size, again, is not small enough to have the stress contours change reliably in the vicinity of the refractory and slag coating.

Areas of maximum stress in ring #1 are within the lands and below the grooves. During coal flow, the principal stresses within the lands increases from 120,000 N/cm^2 to 150,000 N/cm^2. The lands are of less structural importance, acting more as a protective region for the ring, so that the stresses below the grooves are of more importance. Nearly constant stresses of 100,000 N/cm^2 are predicted below the grooves for both oil and coal flows.

Further down the channel, ring #31 is still experiencing high compressive stresses. During the transition form oil to coal combustion, maximum principal stresses in the lands increase from about 60,000 N/cm^2 to 120,000 N/cm^2. Principal stresses below the grooves increase from 60,000 N/cm^2 to 100,000 N/cm^2.

Stresses that are well above the ultimate strength of the stainless steel are indicated. The stresses predicted by the finite element analysis are most likely high due to the thermally induced compression. As previously mentioned, though, it is possible that a portion of the thermal stresses are relieved by such effects as work-hardening or relaxation, i.e. plastic behavior.

A cylinder in compression would possibly exhibit a higher ultimate strength than a flat plate compressed along its edges. The cooling-water passage dividers might also act as stiffeners, again increasing the ring's resistance to buckling or failure. Ring #31 with no dividers has a significant increase in maximum stresses, although a comparison with the other rings is difficult since this ring experiences a much greater relative increase in heat flux.

Thermal cycling is a likely mode of failure due to the high stress levels. Plastic deformation during running conditions may place the rings in tension when cooled. Cracks could possibly appear from the sharp corners of the grooves since high stresses exist in those areas.

CHAPTER IX

RECOMMENDATIONS

Design of future inner rings should incorporate the water-cooling passage dividers not only to aid in uniform water flow but also to increase the stiffness of the ring. The dividers of the throat ring and ring #1 appear to be a factor in the reduction of stresses. The square grooves could provide a starting point for failure when the rings cool. For this reason, the introduction of rounded grooves is recommended. The depth of the grooves might also be reduced to help introduce a more uniform temperature distribution. The complete removal of the grooves might prove impractical in light of other experimental flow characteristics required. Perhaps the use of a material with a smaller coefficient of thermal expansion would help to reduce the stresses.

The high stresses involved might possibly suggest a elastic-plastic analysis in more detail than this study. Other studies might be conducted including the liquid slag layer present with convective heat transfer at these areas. The possible melting or breaking off of both the refractory and the slag layer has significant influence on the heat transfer through the rings which, therefore, has a direct influence on the stresses present. Finally, it is recommended that efforts be made to accurately determine the heat flux to the cooling rings at the same time thermocouple temperatures are determined. Based on the experimental values from previous tests, the predicted ring temperatures are not consistent with the experimentally measured temperatures, but are consistent with the applied heat flux values. The measured temperatures are not consistent with the measured heat flux values.

LIST OF REFERENCES

LIST OF REFERENCES

1. "Management Plan for MHD Research & Development and Operation of the MHD Coal Fired Flow Facility (CFFF)." The University of Tennessee Space Institute. 1987.

2. Brick, Robert M.; Gordon, Robert B.; and Phillips, Arthur. Structure and Properties of Alloys. 3rd Ed. New York: McGraw-Hill Book Co., 1965.

3. Shaver, T., unpublished data. The University of Tennessee Space Institute, Energy Conversion Research and Development Programs. Tullahoma, Tennessee, 1987.

4. Rodgers, M.E., and Kruger, C.H. "Fluid Mechanics and Thermal Behavior of MHD Channel Slag Layers." 17th Symposium on Engineering Aspects of MHD. Stanford, California: Stanford University, 1978.

5. Schulz, R., unpublished data. The University of Tennessee Space Institute, Energy Conversion Research and Development Programs. Tullahoma, Tennessee, 1987.

6. McMinn, W., unpublished data. The University of Tennessee Space Institute, Energy Conversion Research and Development Programs. Tullahoma, Tennessee, 1987.

7. Fenech, H., and Rohsenow, W.M. "Prediction of Thermal Conductance of Metallic Surfaces in Contact." ASME Transactions: Journal of Heat Transfer. Vol. 85 (February, 1963).

8. Barzelay, Martin E.; Tong, Kin Nee; and Hollo, George. "Thermal Conductance of Contacts in Aircraft Joints." NACA Technical Note 3167. Washington D.C.: March, 1954.

9. Manson, S.S. "Behavior of Materials under Conditions of Thermal Stress." NACA Technical Note 1170. Washington D.C.: 1954.

10. Boyer, Howard E., Ed. Metals Handbook. Vol. 10: Failure Analysis and Prevention. Metals Park, Ohio: American Society for Metals, 1975.

11. Galletly, G.D., and Pemsing, K. "On Design Procedures for the Buckling of Cylinders Under Combined Axial Compression and External Pressure." Journal of Pressure Vessel Technology. Vol. 106, May, 1984.

12. Bushnell, D., and Meller, E. "Elastic-Plastic Collapse of Axially Compressed Cylindrical Shells: A Brief Survey With Particular Application to Ring-Stiffened Cylindrical Shells With Reinforced Openings." Journal of Pressure Vessel Technology. Vol. 106, February, 1984.

13. Donnell, Lloyd Hamilton. Beams, Plates, and Shells. New York: McGraw-Hill Book Co., 1976.

14. Lubahn, J.D., and Felgar, R.P. Plasticity and Creep of Metals. New York: John Wiley and Sons, Inc., 1961.

15. Zeinkiewicz, O.C. The Finite Element Method. London: McGraw-Hill Book Co., Ltd., 1977.

16. Dhatt, Gouri, and Touzot, Gilbert. The Finite Element Method Displayed. Chicester: John Wiley and Sons, 1984.

17. Desai, Chandrakant S., and Abel, John F. Introduction to the Finite Element Method, A Numerical Method for Engineering Analysis. New York: Van Nostrand Reinhold Co., 1972.

Supplementary References

Arpaci, Vedat S. Conduction Heat Transfer. Reading, Mass.: Addison-Wesley Publishing Co., 1966.

Barber, J.R. "The Influence of Interface Thermal Contact Resistance on the Heat Transfer Performance of Prestresses Duplex Tube." International Journal of Heat and Mass Transfer. Vol. 29, (1986), pp. 761-767.

Baumeister, Theodore, Ed. Standard Handbook for Mechanical Engineers. 7th Ed. New York: McGraw-Hill Book Co., 1967.

Fenech, Henri. "Thermal Conductance at Solid Interfaces: An Application of the Fenech-Rohsenow Model." International Journal of Heat and Mass Transfer. Vol. 29, (1986), pp. 1103-1108.

Ford, Hugh. Advanced Mechanics of Materials. New York: John Wiley and Sons, Inc., 1963.

Fritz, R.J. "Evaluation of Transient Temperatures and Stresses." Transactions of the ASME. Vol. 76, (1954), pp. 913-921.

Goodier, J.N. "Thermal Stress and Deformation." Transactions of the ASME: Journal of Applied Mechanics. Vol. 79 (1957), pp. 467-474.

Hoffman, Peter L.R. "Heat Transfer Studies of Magnetohydrodynamic Power Train Components." Master's Thesis, The University of Tennessee Space Institute. 1984.

Huebner, Kenneth H. The Finite Element Method for Engineers. New York: John Wiley and Sons, Inc., 1975.

Kreith, Frank. Principles of Heat Transfer. 3rd Ed. New York: Intext Educational Publishers, 1973.

Nakamura, Shocchiro. Computational Methods in Engineering and Science, With Applications to Fluid Dynamics and Nuclear Systems. New York: John Wiley and Sons, Inc., 1977.

Polakowski, N.H., and Ripling, E.J. Strength and Structure of Engineering Materials. Englewood Cliffs, New Jersey: Prentice-Hall, Inc., 1966.

Timoshenko, S.P., and Goodier, J.N. Theory of Elasticity. New York: McGraw-Hill Book Co., 1934.

Whittaker, Stephen. Elementary Heat Transfer Analysis. New York: Pergamon Press Inc., 1976.

APPENDIX

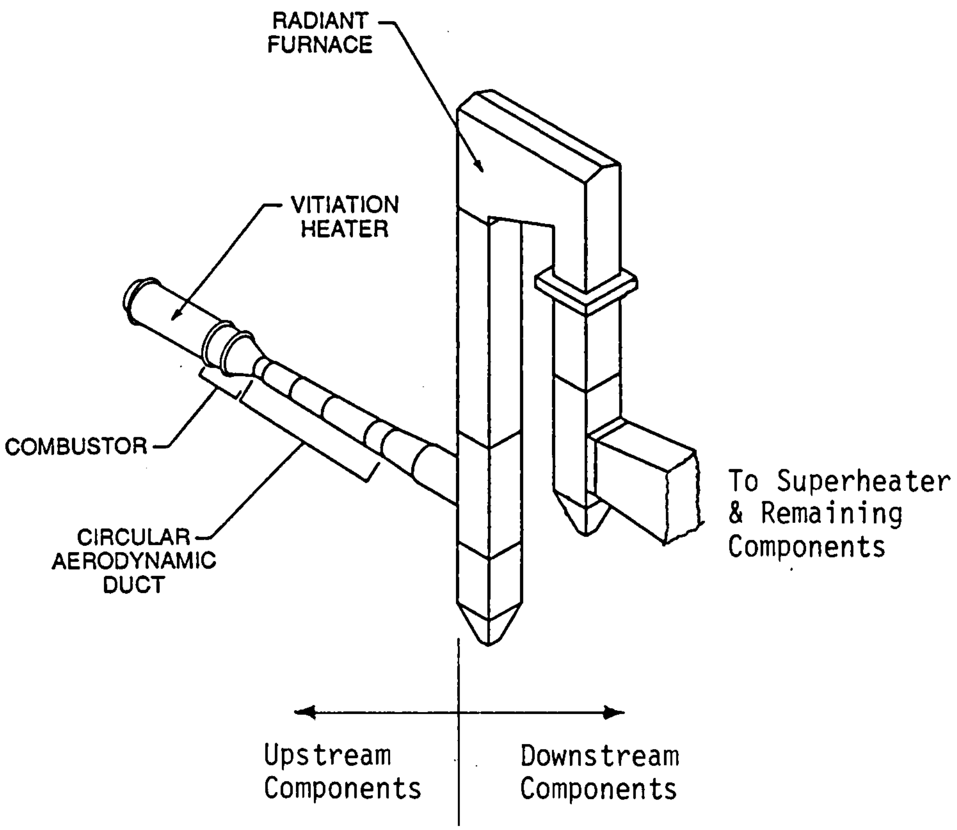

Figure 1. Schematic of Upstream Components of the Coal Fired Flow Facility

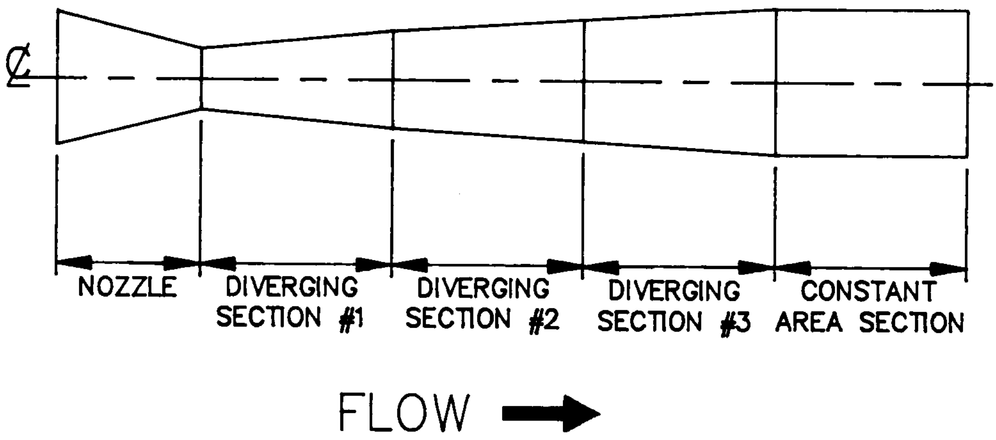

Figure 2. Nozzle and Circular Aerodynamic Duct

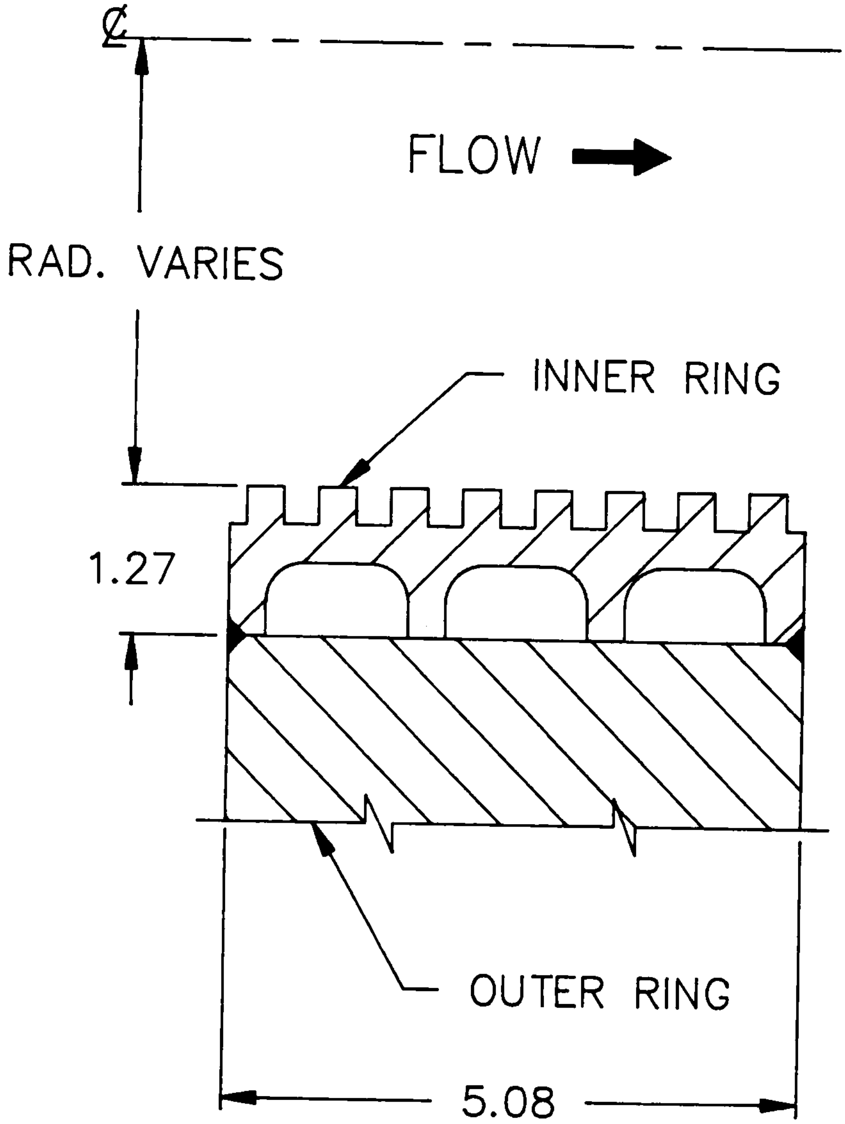

Figure 3. Typical Weldment of Inner and Outer Rings

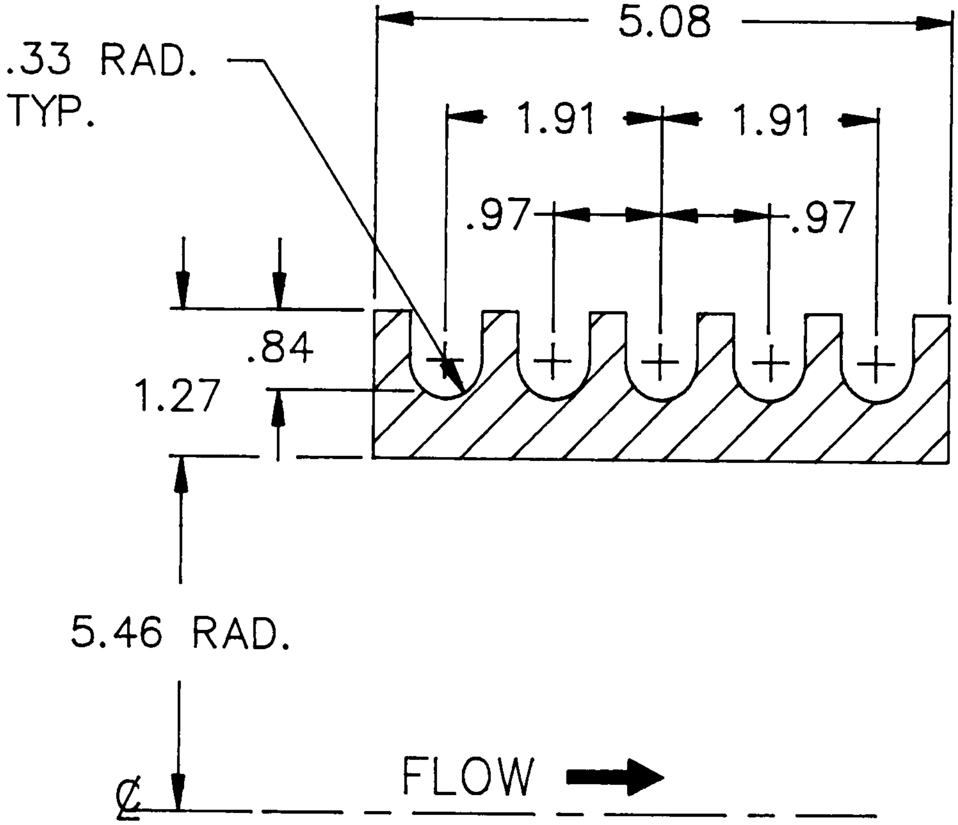

Figure 4. Cross-Section of Inner Throat Ring of Nozzle

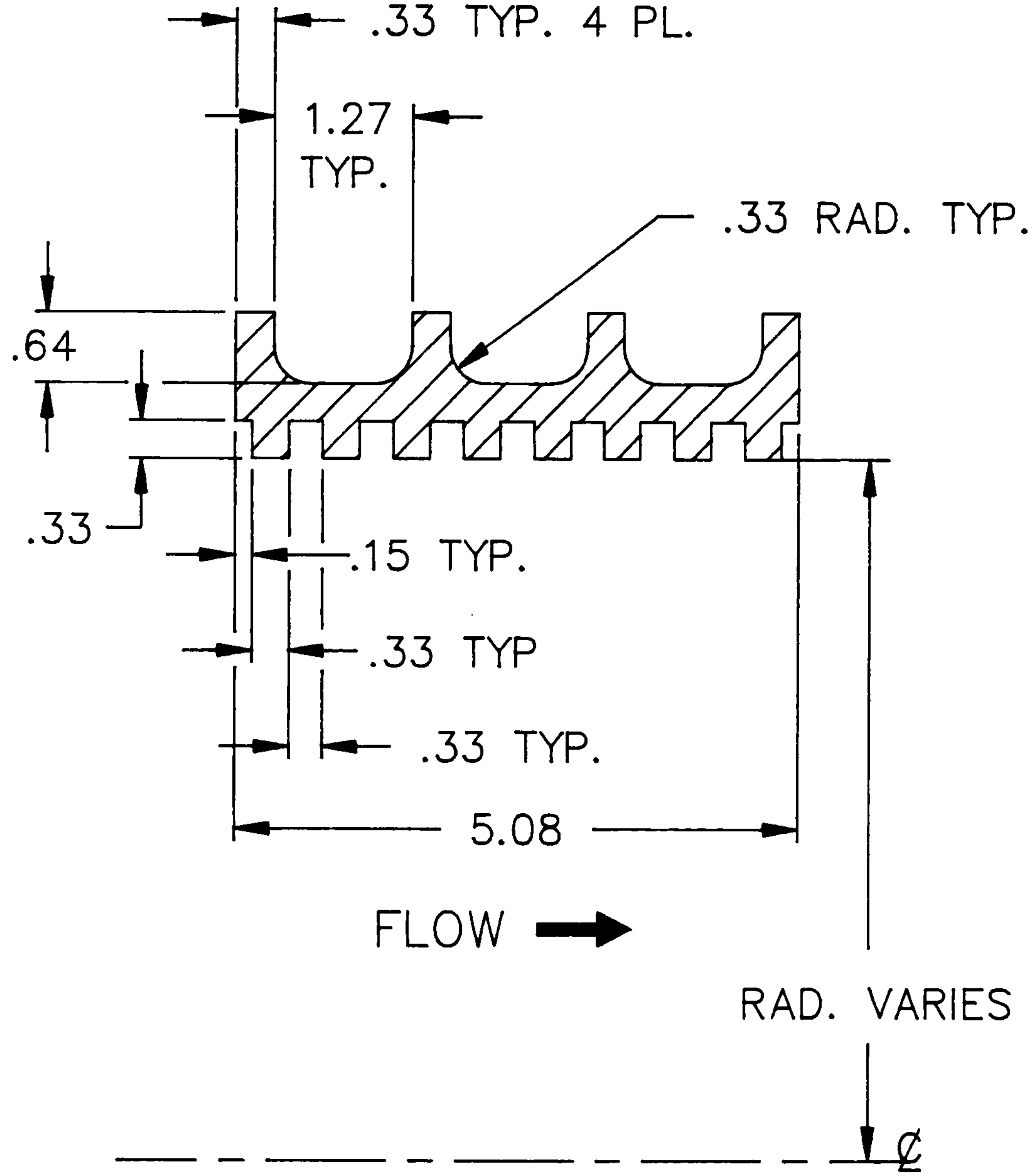

Figure 5. Typical Cross-Section of Inner Ring of Circular Duct Sections #1 and #2

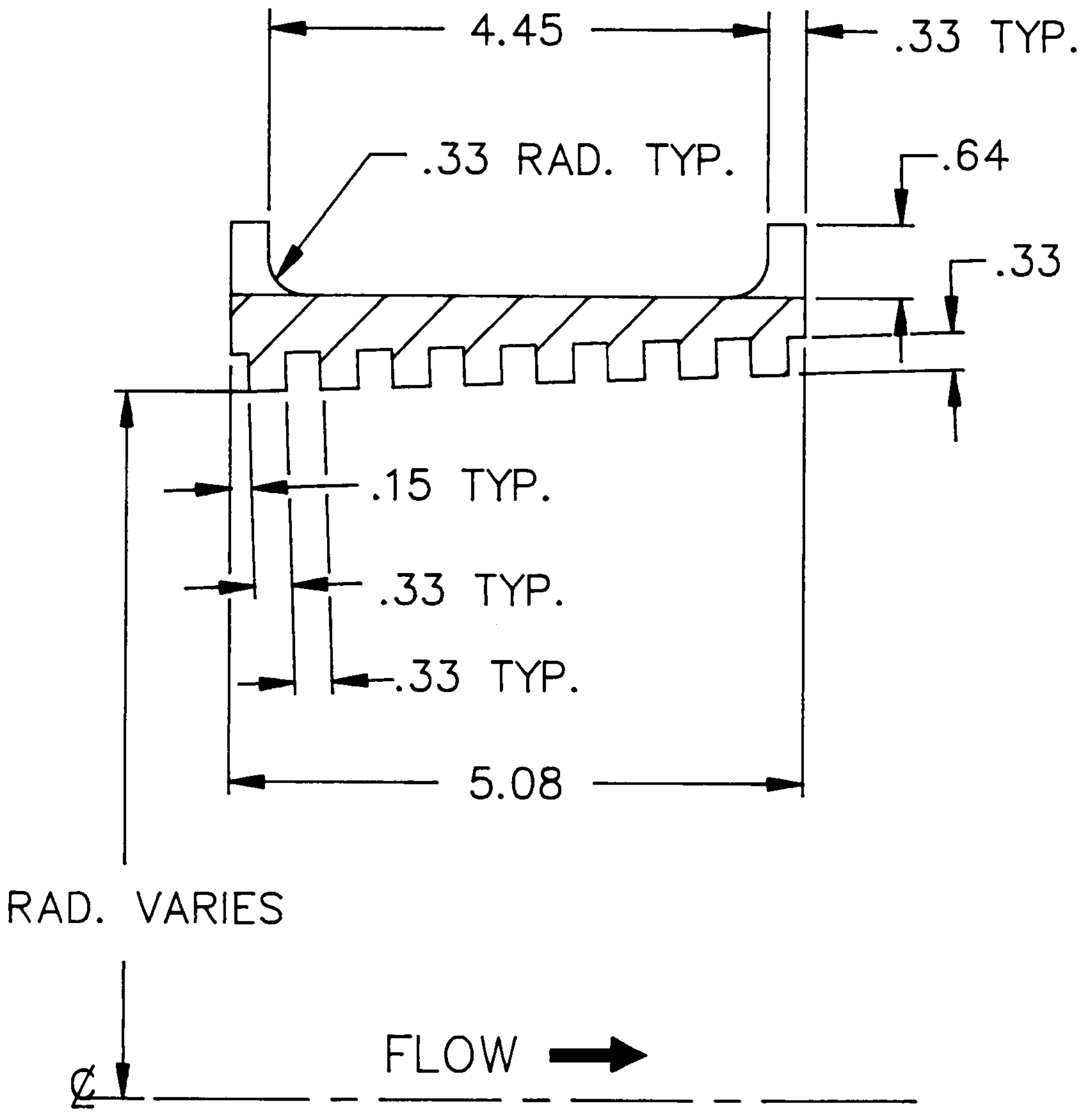

Figure 6. Typical Cross-Section of Inner Ring of Circular Duct Section #3

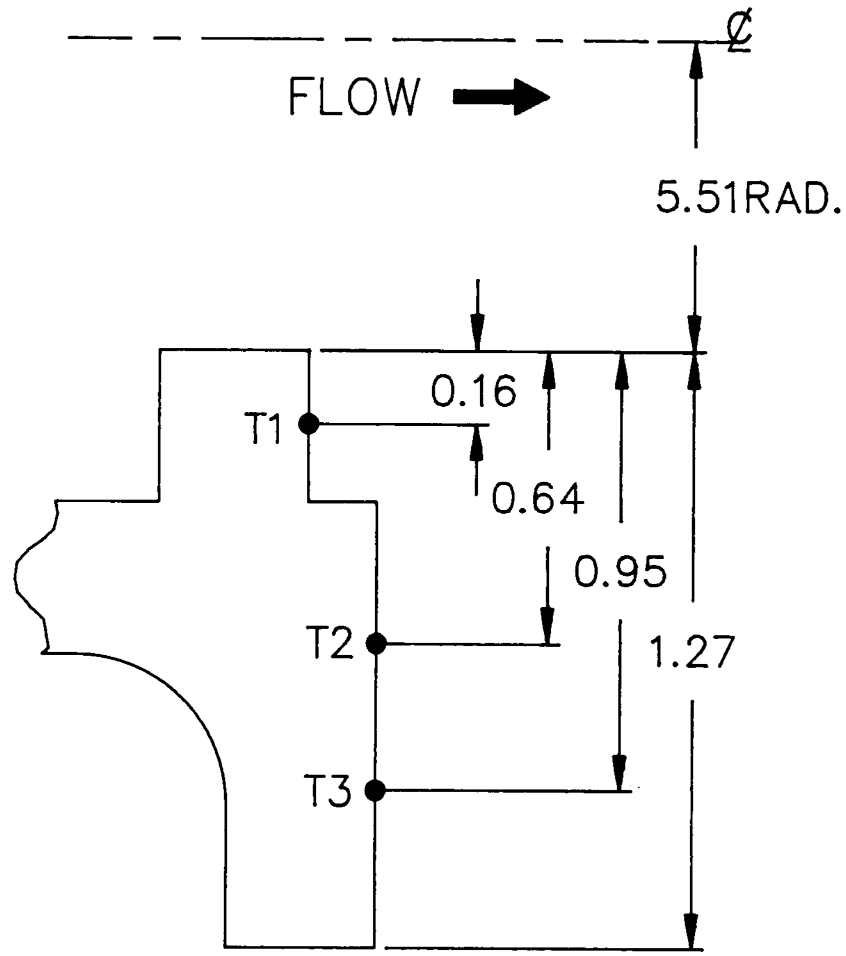

Figure 7. Thermocouple Placement on Ring #1 of Section #1

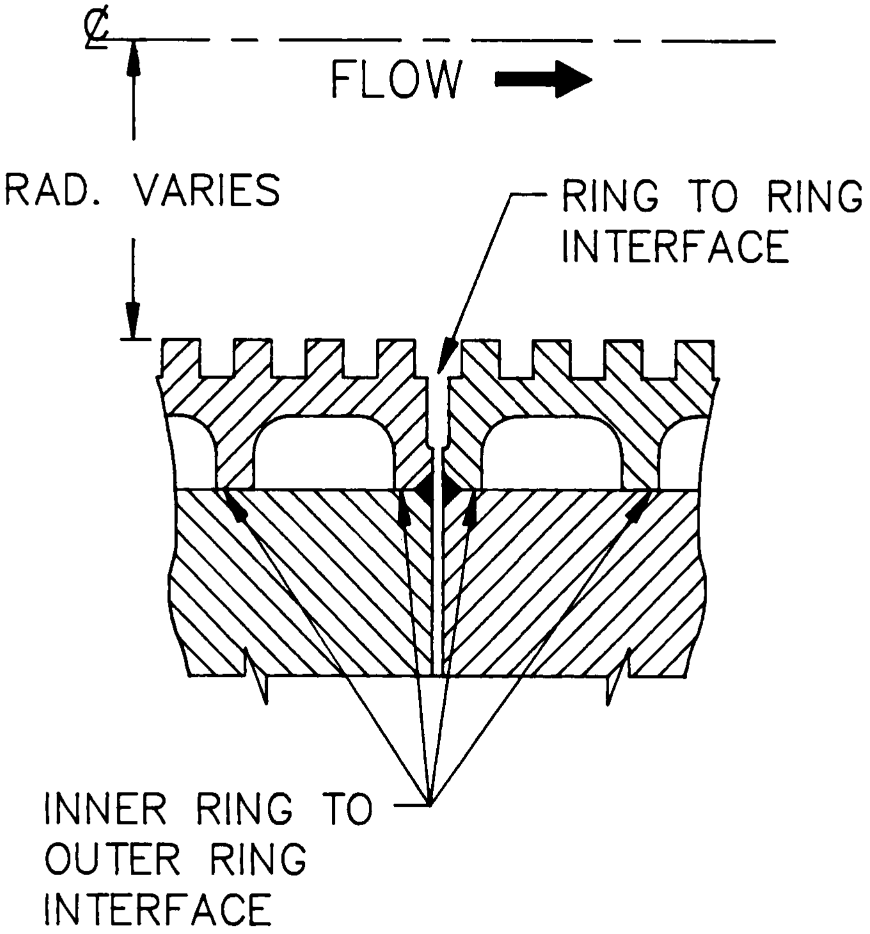

Figure 8. Areas of Contact Resistance Between Rings

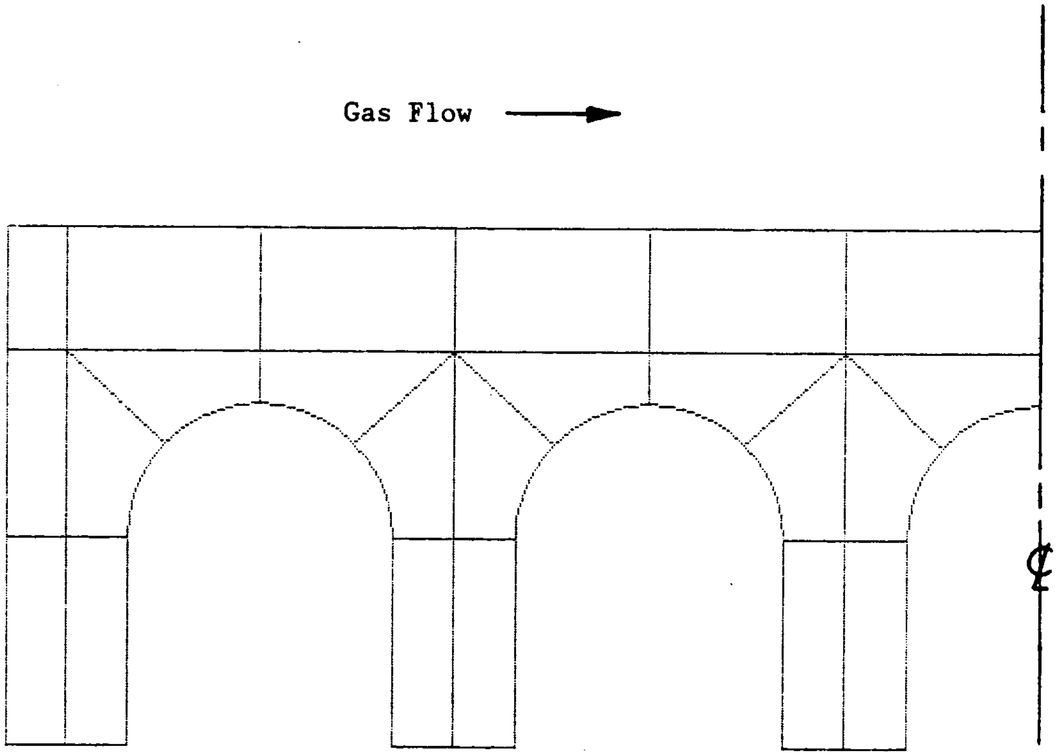

Figure 9. Throat Ring, Oil Flow Model

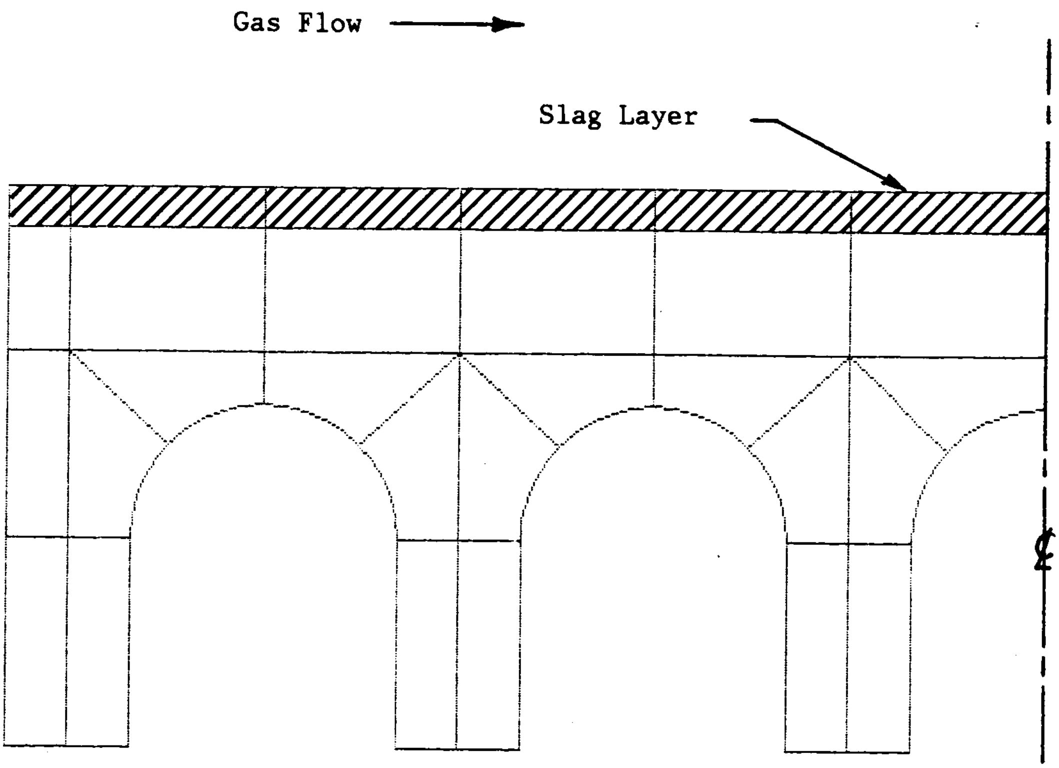

Figure 10. Throat Ring, Coal Flow Model

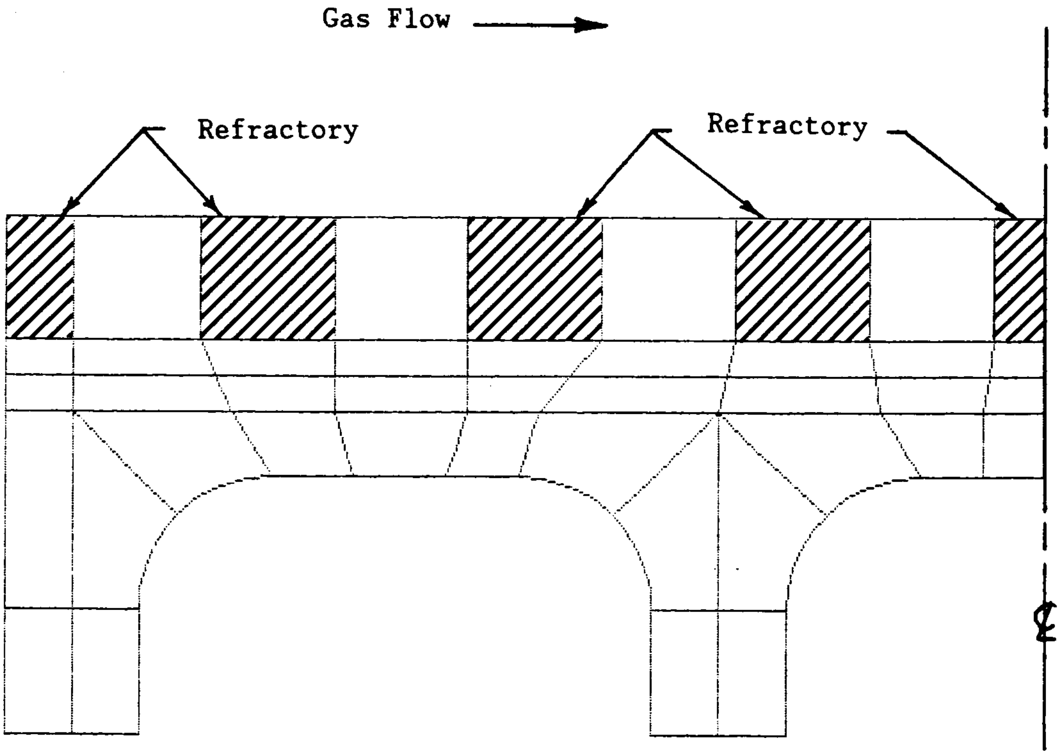

Figure 11. Ring #1, Oil Flow Model

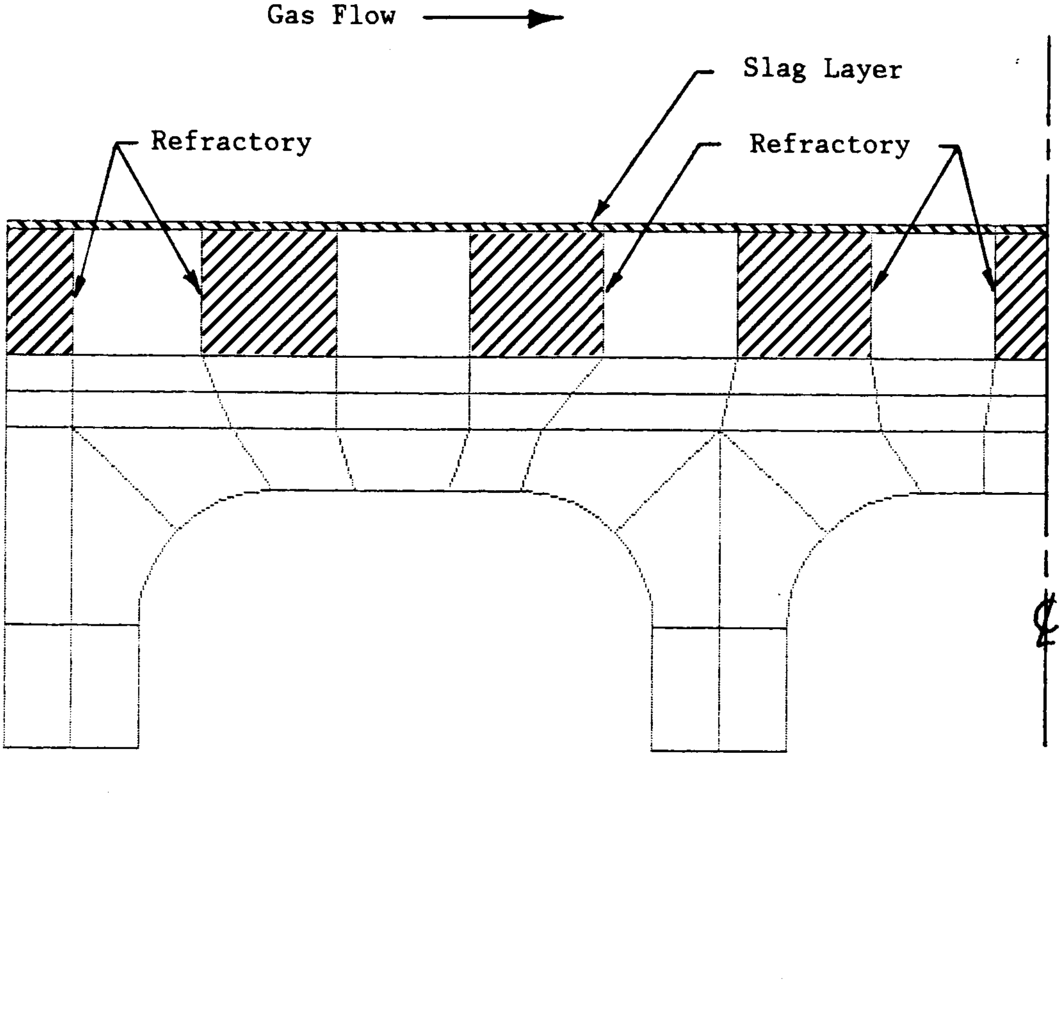

Figure 12. Ring #1, Coal Flow Model

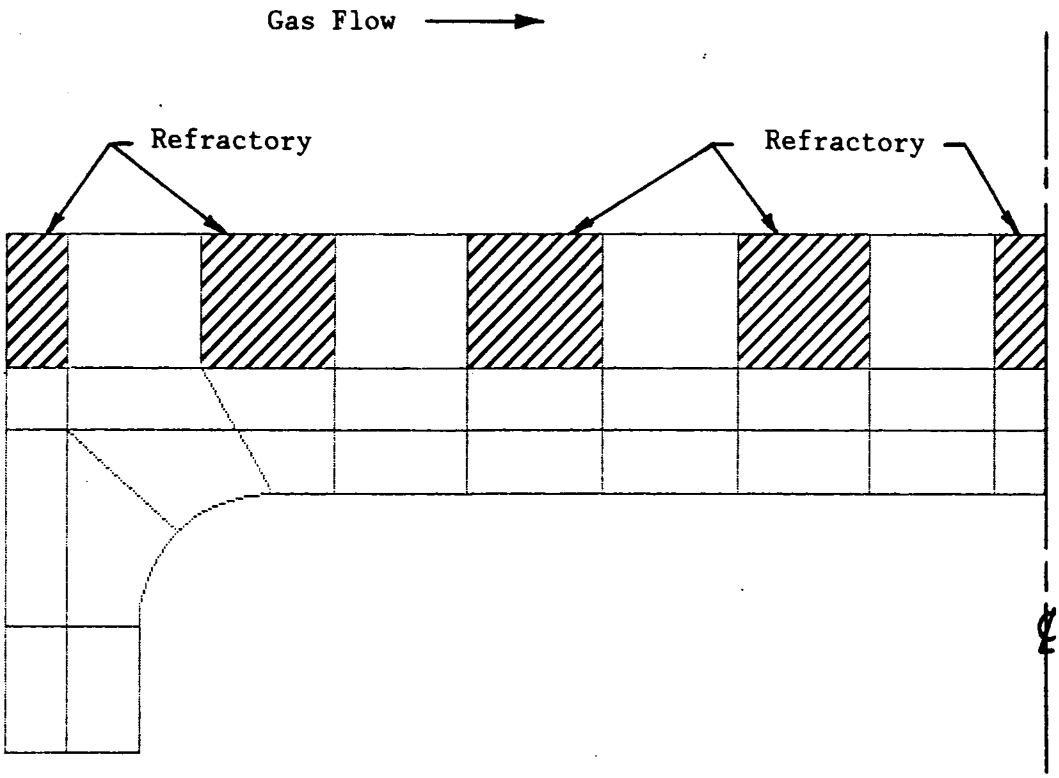

Figure 13. Ring #31, Oil Flow Model

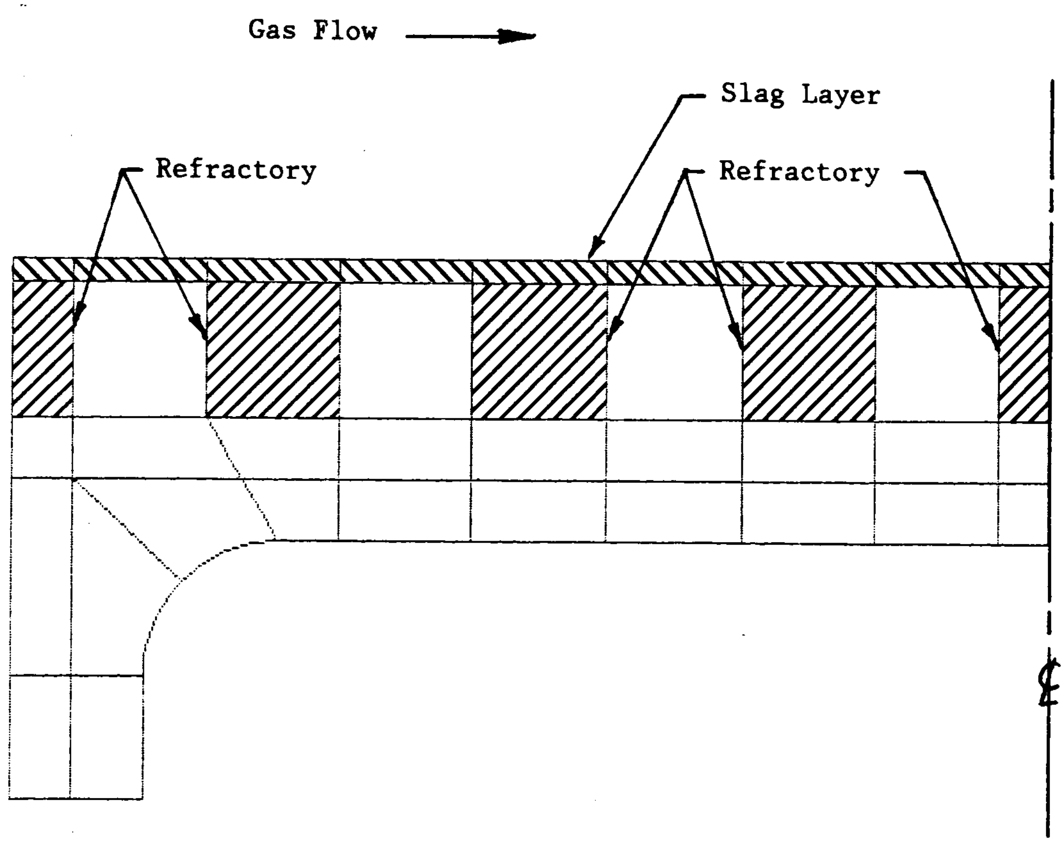

Figure 14. Ring #31, Coal Flow Model

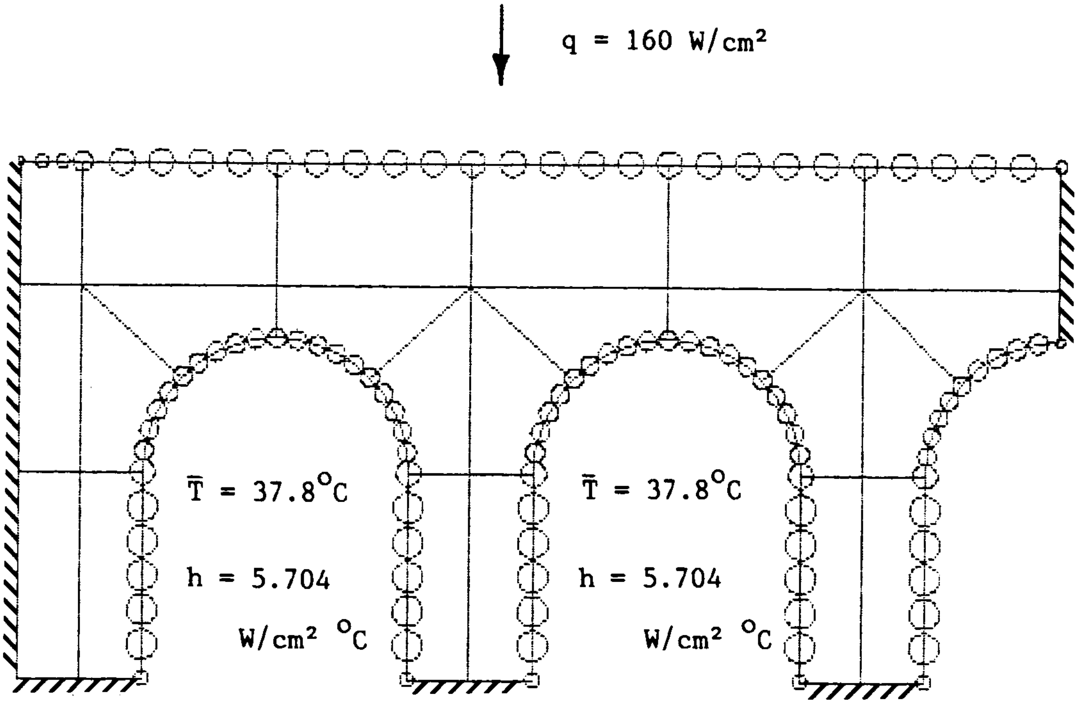

Figure 15. Throat Ring, Thermal Boundary Conditions (Oil)

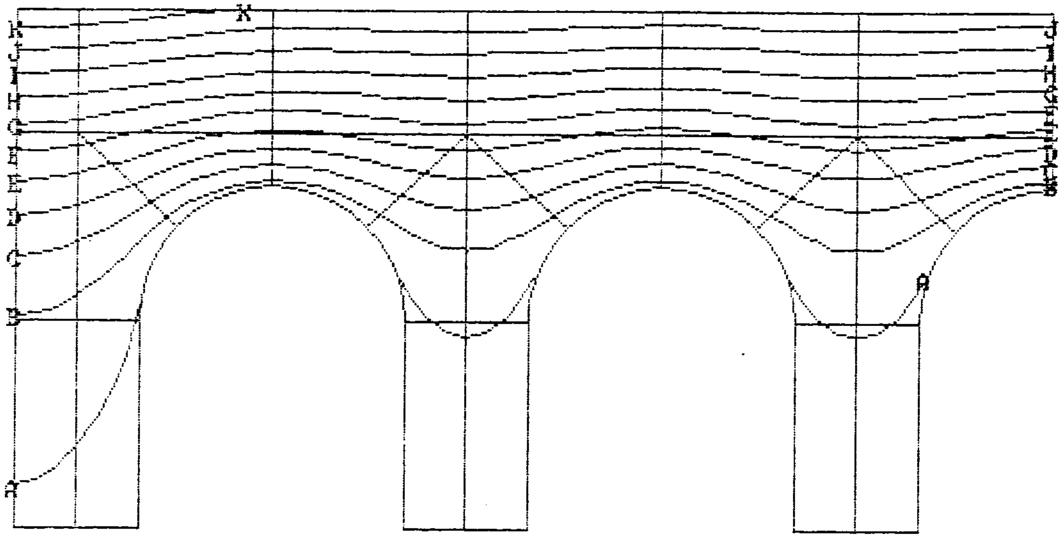

Temperatures (°C)

A	50.0
B	100.0
C	150.0
D	200.0
E	250.0
F	300.0
G	350.0
H	400.0
I	450.0
J	500.0
K	550.0

Figure 16. Throat Ring, Isotherms (Oil)

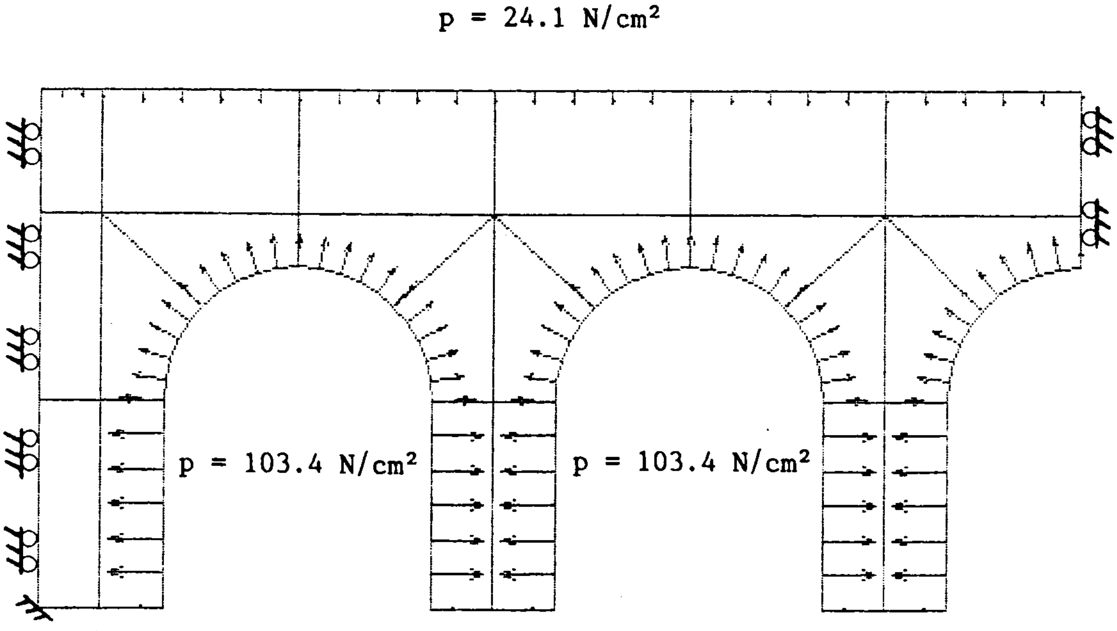

Figure 17. Throat Ring, Pressure Loads and Constraints (Oil)

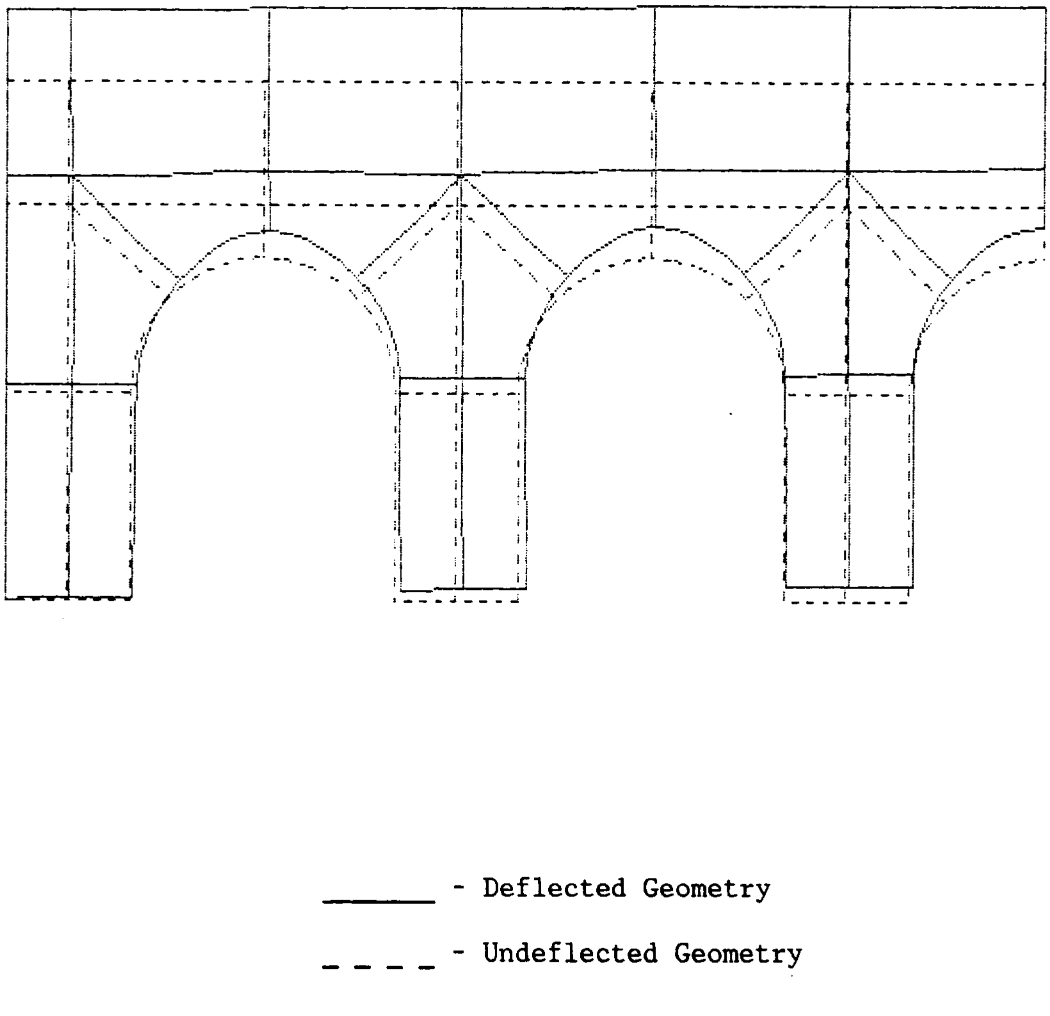

Figure 18. Throat Ring, Deflections (Oil)

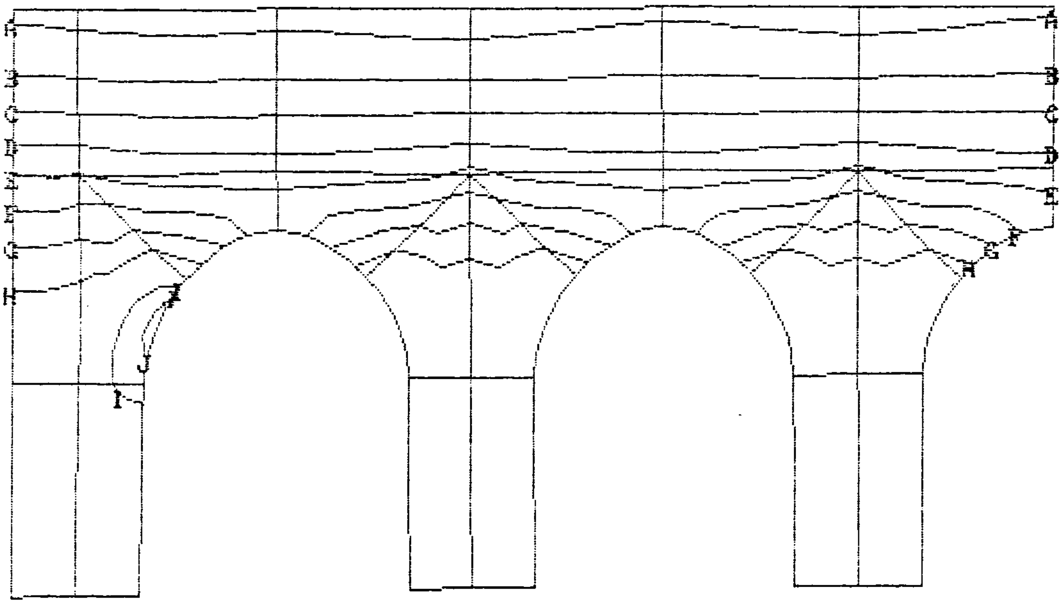

Maximum Principle
Stresses (N/cm^2)

A	-1.6E+05
B	-1.4E+05
C	-1.2E+05
D	-1.0E+05
E	-8.0E+04
F	-6.0E+04
G	-4.0E+04
H	-2.0E+04
I	1.0E+04
J	2.0E+04

Figure 19. Throat Ring, Maximum Principal Stresses (Oil)

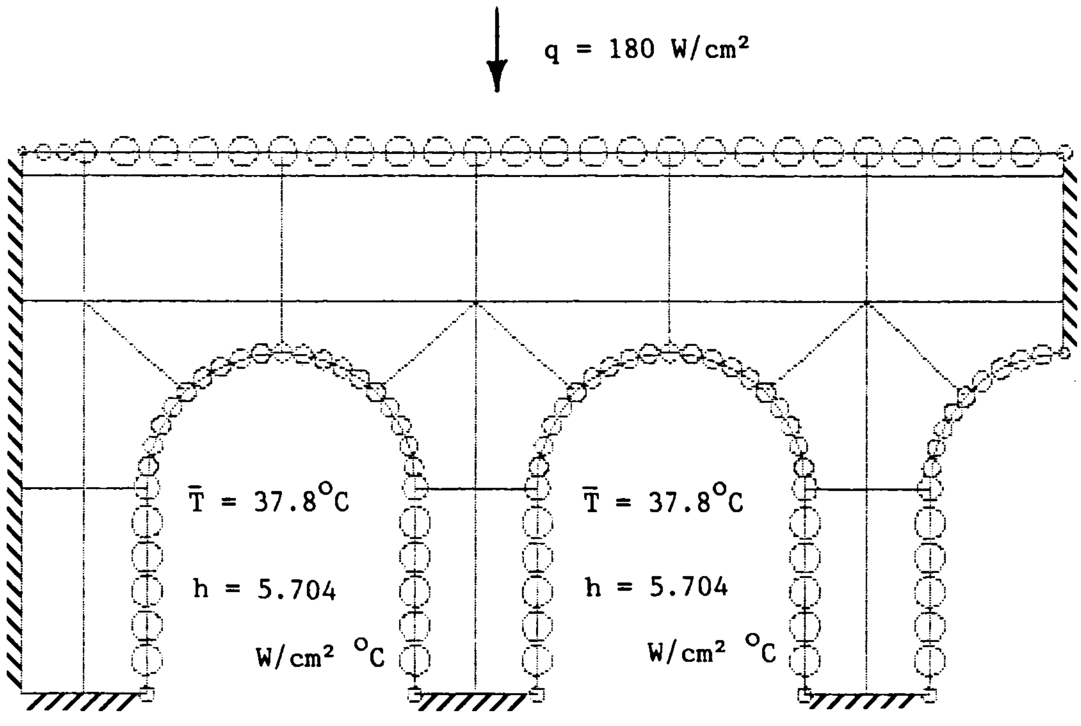

Figure 20. Throat Ring, Thermal Boundary Conditions (Coal)

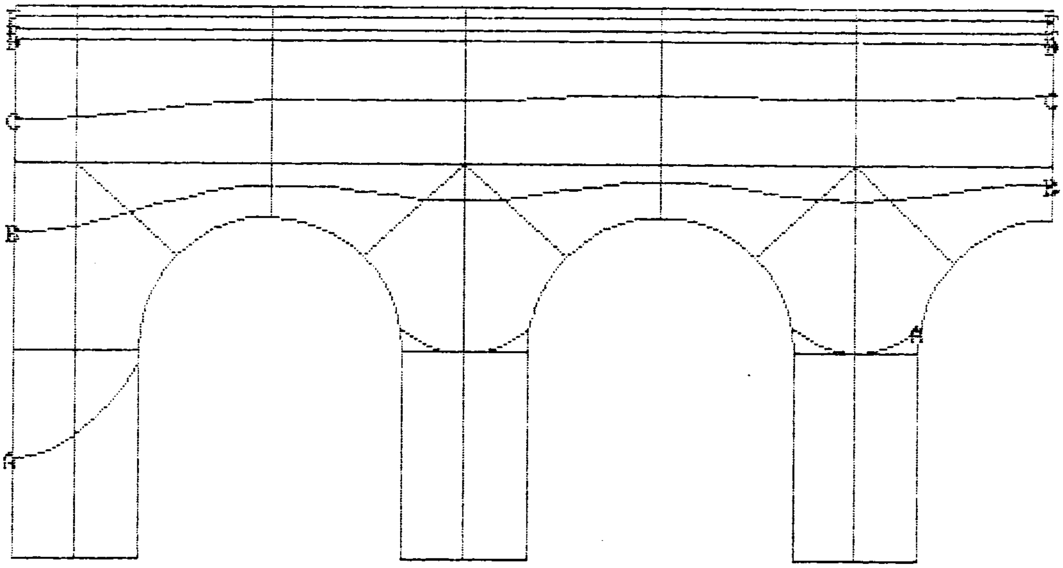

Temperatures ($^{\circ}C$)

A	50.0
B	100.0
C	150.0
D	200.0
E	500.0
F	1000.0

Figure 21. Throat Ring, Isotherms (Coal)

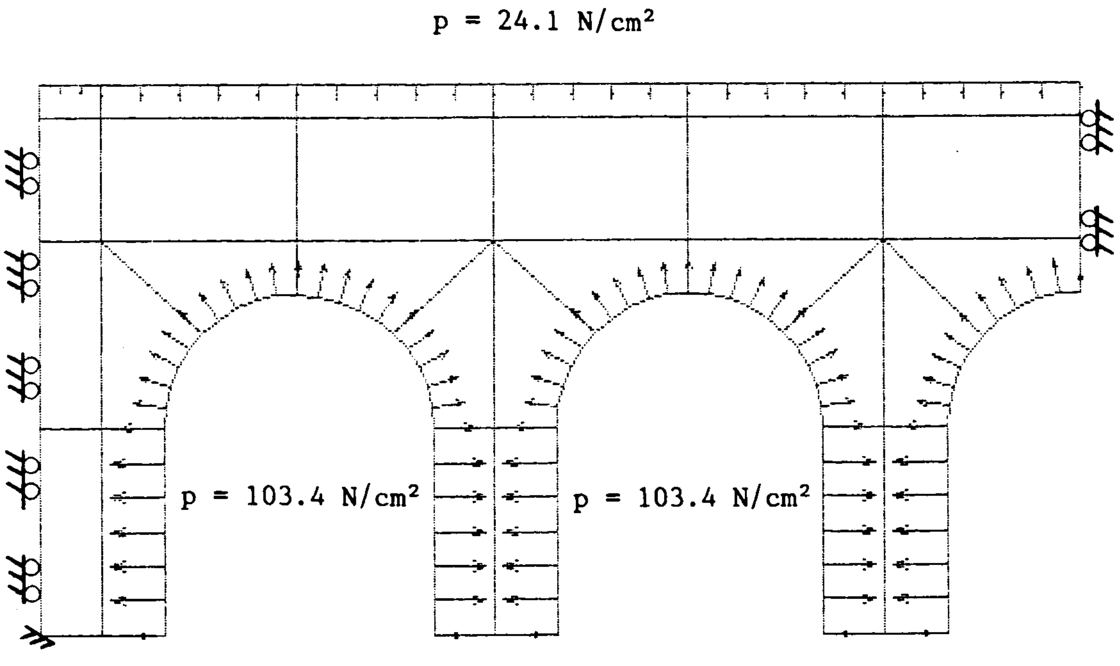

Figure 22. Throat Ring, Pressure Loads and Constraints (Coal)

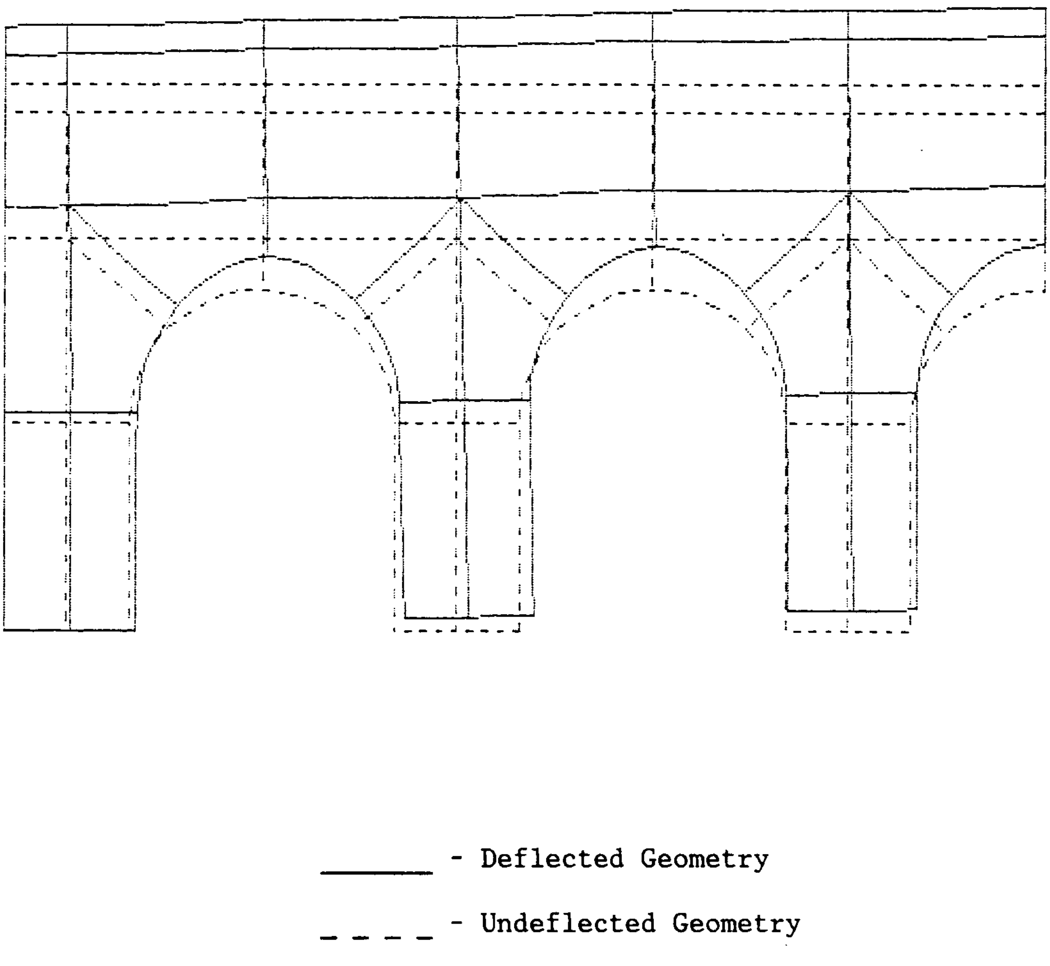

Figure 23. Throat Ring, Deflections (Coal)

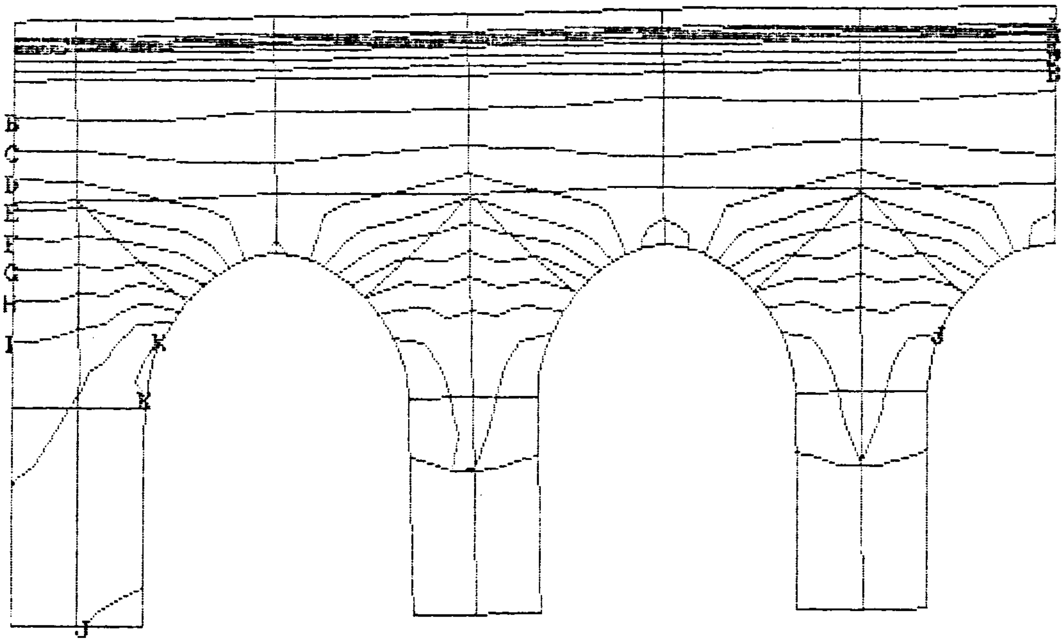

Maximum Principal
Stresses (N/cm^2)

B	-4.0E+04
C	-3.5E+04
D	-3.0E+04
E	-2.5E+04
F	-2.0E+04
G	-1.5E+04
H	-1.0E+04
I	-0.5E+04
J	0.5E+04

Figure 24. Throat Ring, Maximum Principal Stresses (Coal)

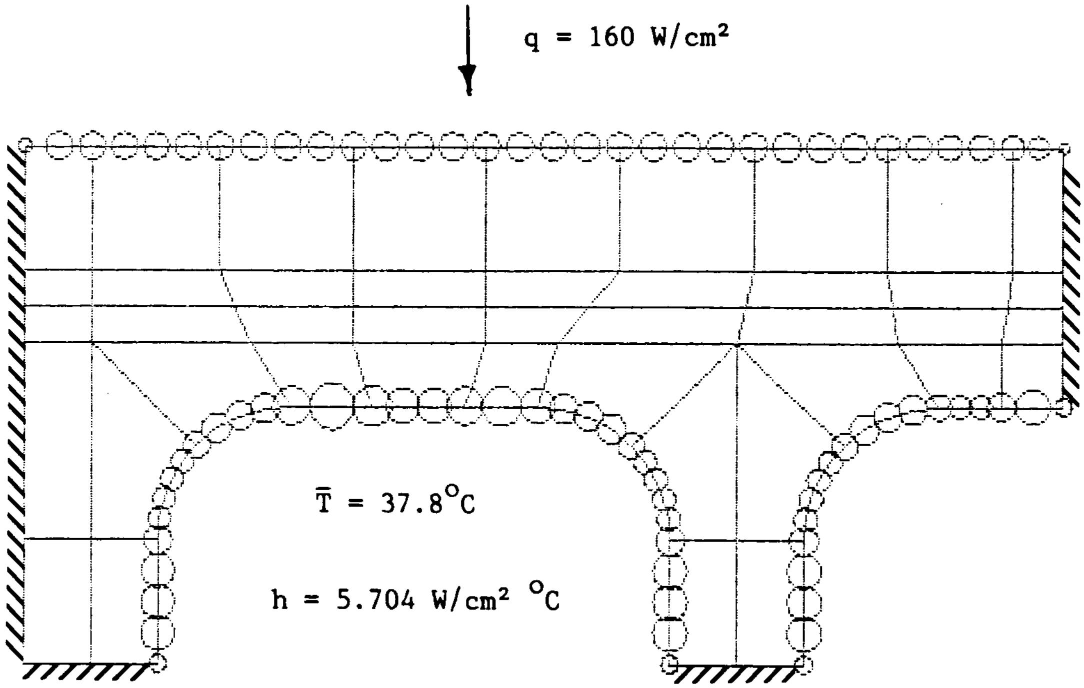

Figure 25. Ring #1, Thermal Boundary Conditions (Oil)

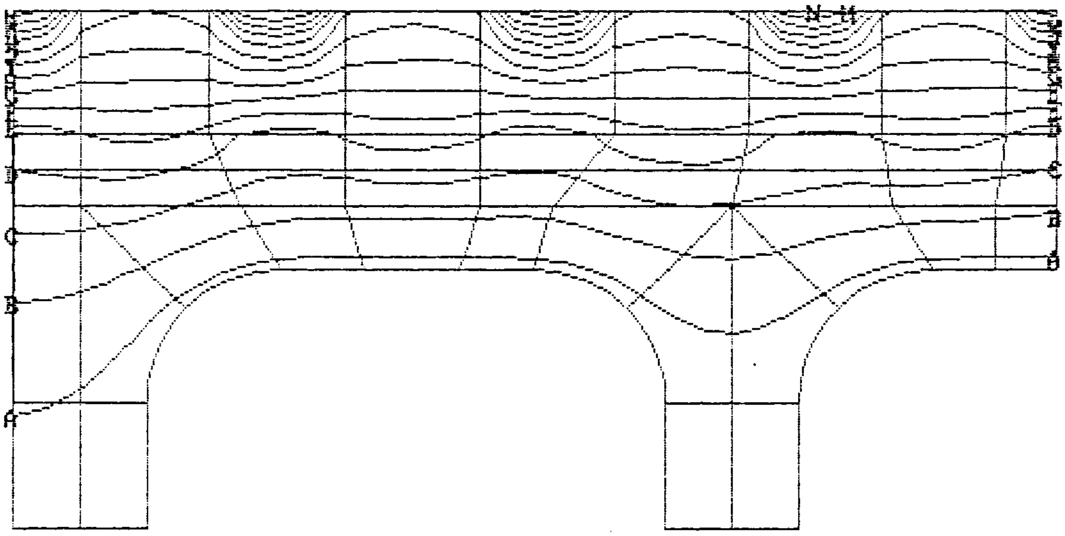

<u>Temperatures (^{o}C)</u>

A	100.0
B	200.0
C	300.0
D	400.0
E	500.0
F	600.0
G	700.0
H	800.0
I	900.0
J	1000.0
K	1100.0
L	1200.0
M	1300.0
N	1400.0

Figure 26. Ring #1, Isotherms (Oil)

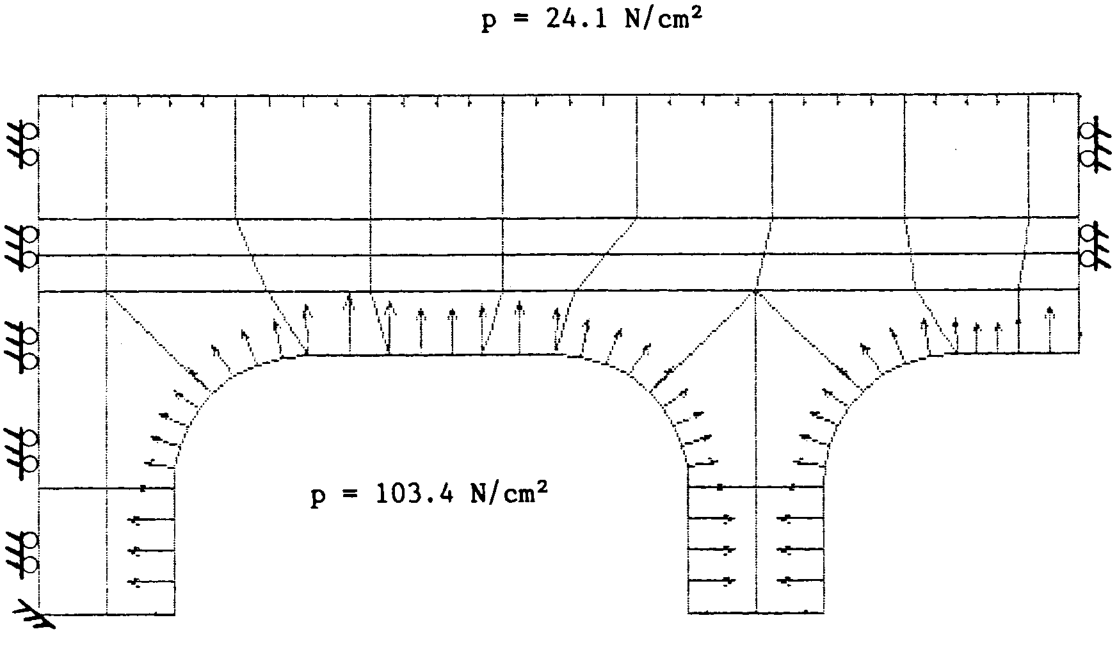

Figure 27. Ring #1, Pressure Loads and Constraints (Oil)

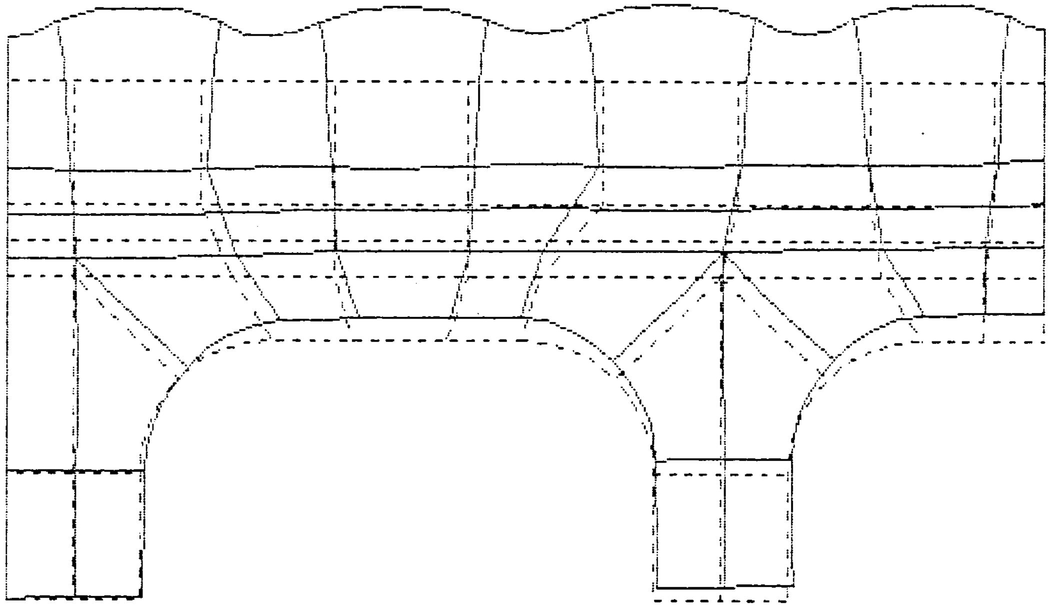

______ - Deflected Geometry

_ _ _ _ - Undeflected Geometry

Figure 28. Ring #1, Deflections (Oil)

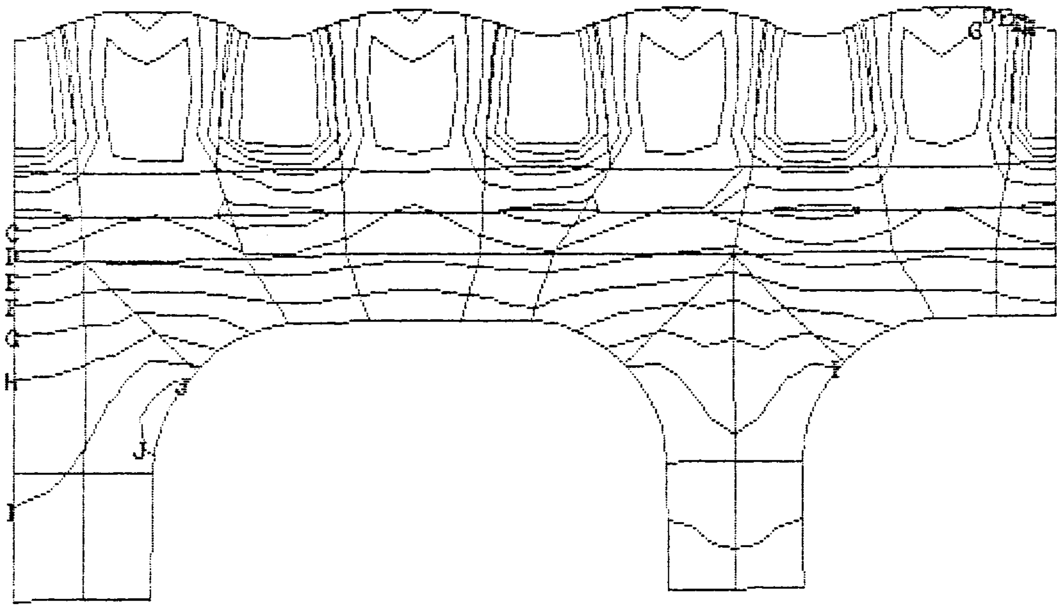

Maximum Principal Stresses (N/cm^2)	
A	-1.6E+05
B	-1.4E+05
C	-1.2E+05
D	-1.0E+05
E	-8.0E+04
F	-6.0E+04
G	-4.0E+04
H	-2.0E+04
I	0.0E+00
J	2.0E+04

Figure 29. Ring #1, Maximum Principal Stresses (Oil)

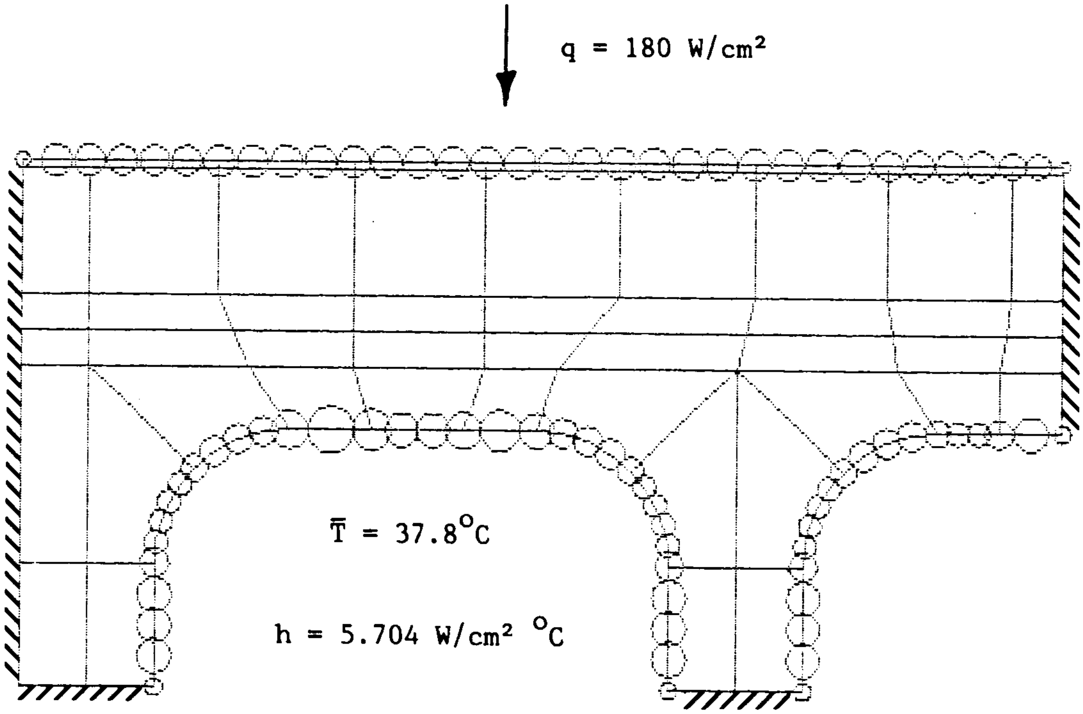

Figure 30. Ring #1, Thermal Boundary Conditions (Coal)

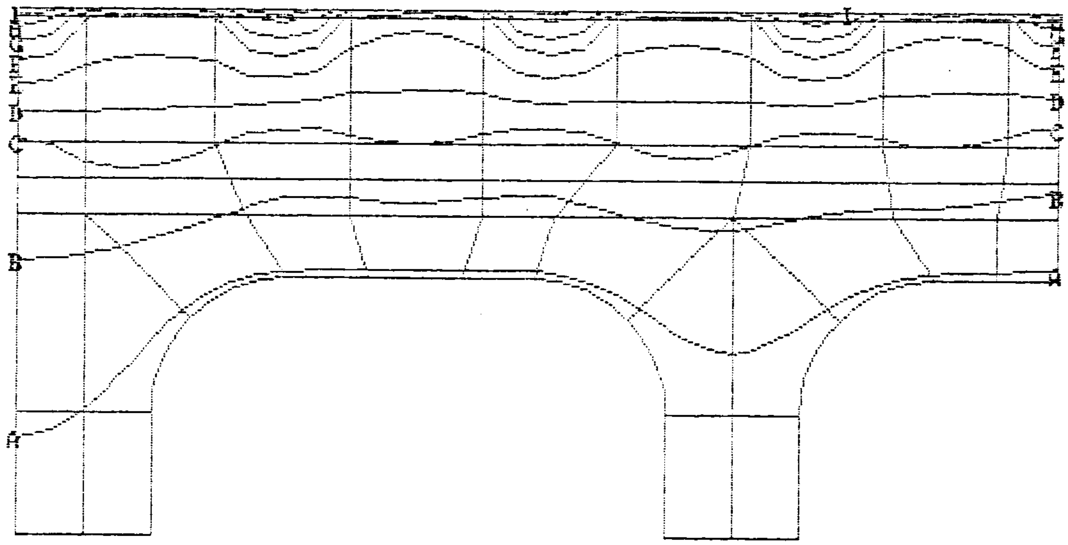

Temperatures (^{o}C)

A	100.0
B	300.0
C	500.0
D	700.0
E	900.0
F	1100.0
G	1300.0
H	1500.0
I	1700.0

Figure 31. Ring #1, Isotherms (Coal)

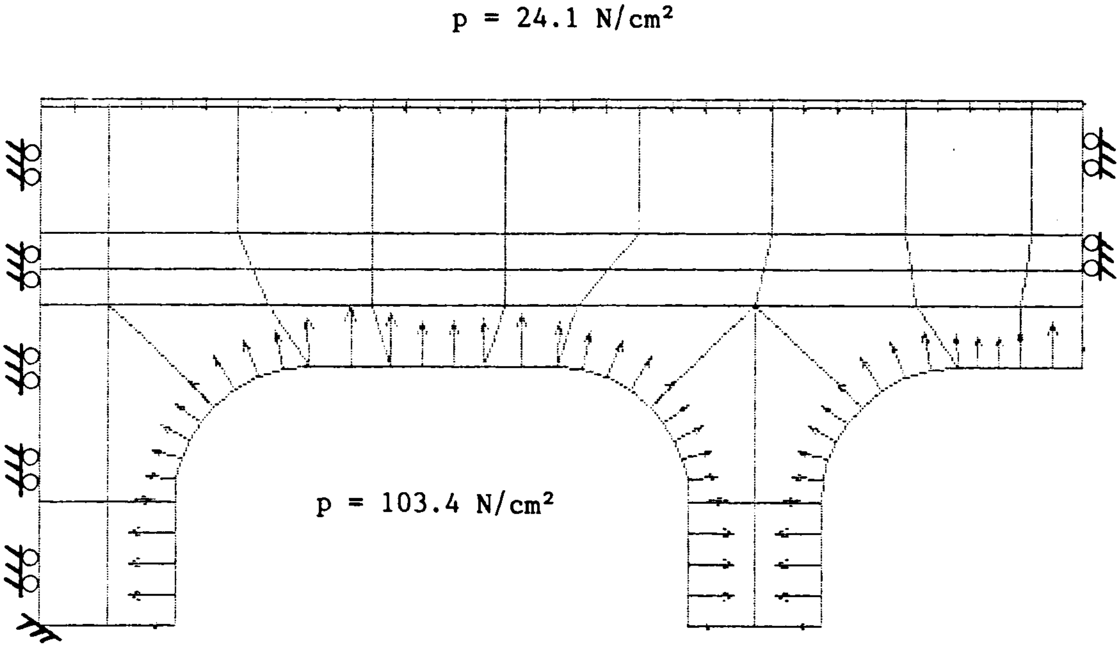

Figure 32. Ring #1, Pressure Loads and Constraints (Coal)

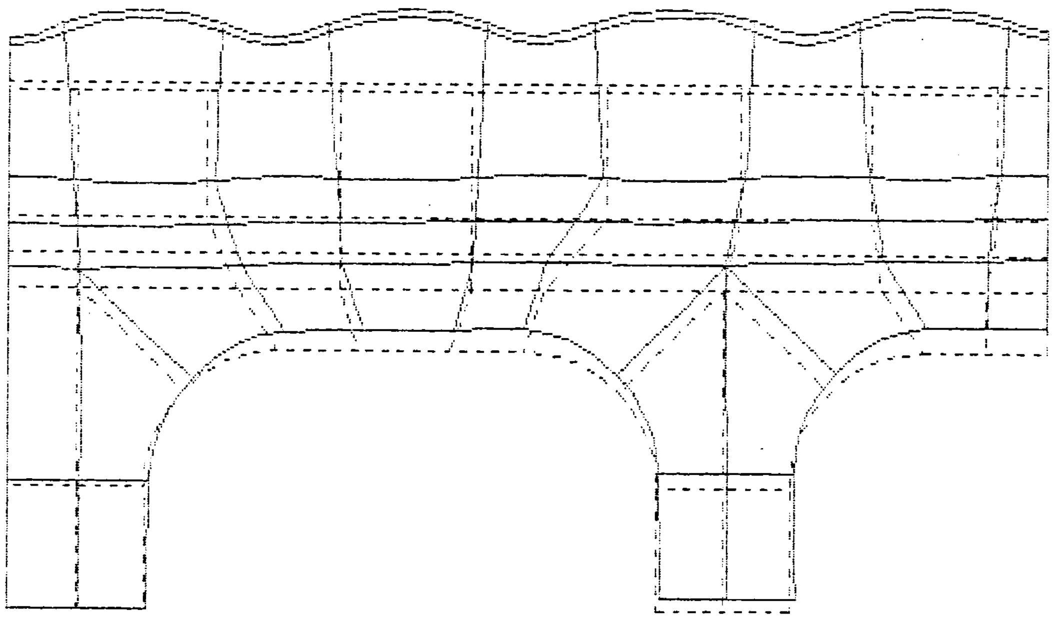

______ - Deflected Geometry

_ _ _ _ - Undeflected Geometry

Figure 33. Ring #1, Deflections (Coal)

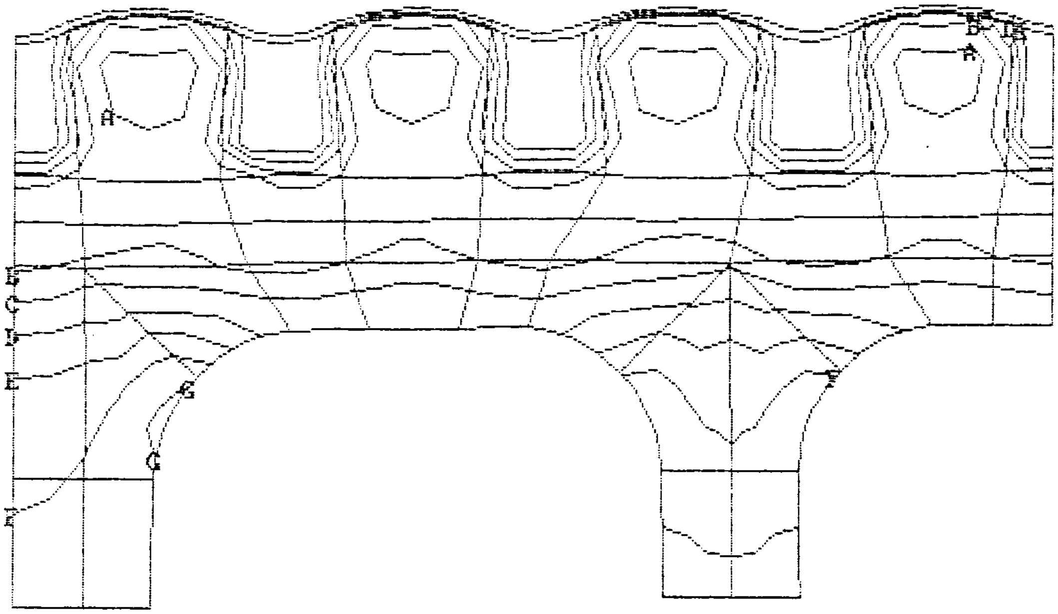

Maximum Principal
Stresses (N/cm²)

A	-1.5E+05
B	-1.0E+05
C	-7.5E+04
D	-5.0E+04
E	-2.5E+04
F	1.0E-03
G	2.5E+04

Figure 34. Ring #1, Maximum Principal Stresses (Coal)

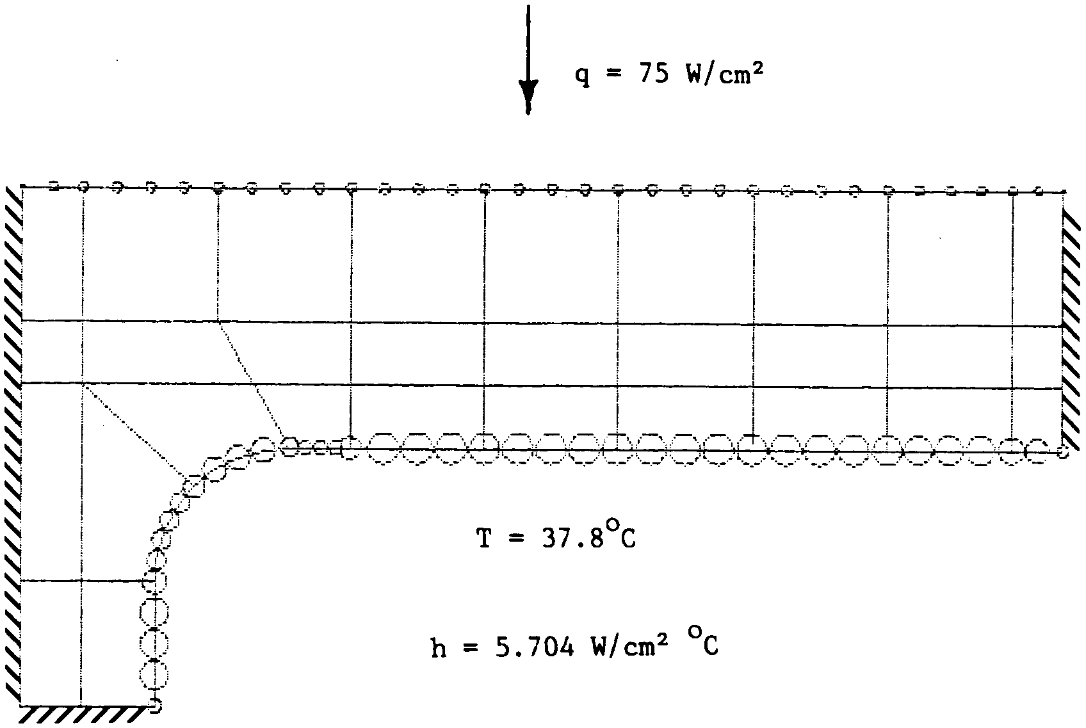

Figure 35. Ring #31, Thermal Boundary Conditions (Oil)

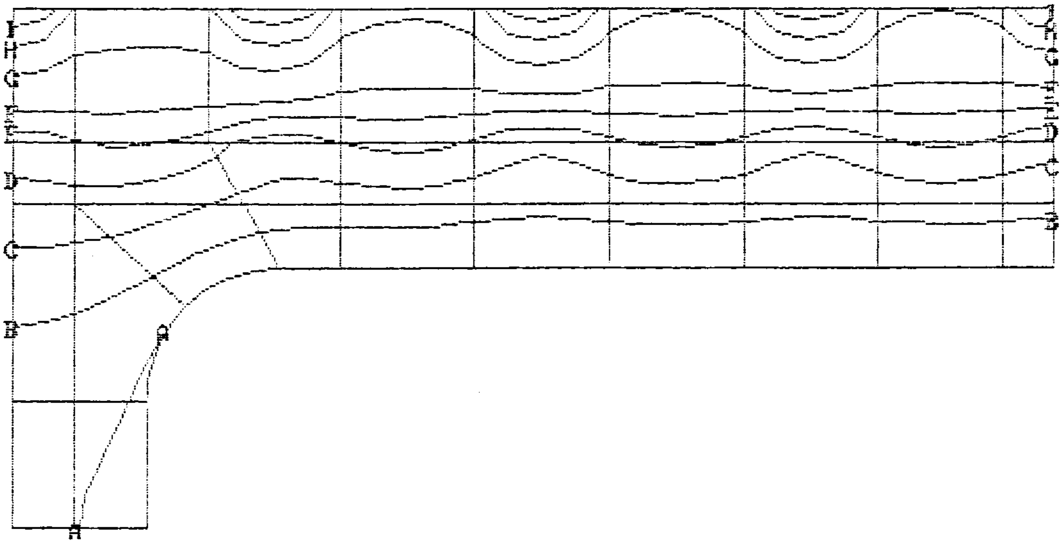

<u>Temperatures (^{o}C)</u>

A	50.0
B	100.0
C	150.0
D	200.0
E	250.0
F	300.0
G	400.0
H	500.0
I	600.0

Figure 36. Ring #31, Isotherms (Oil)

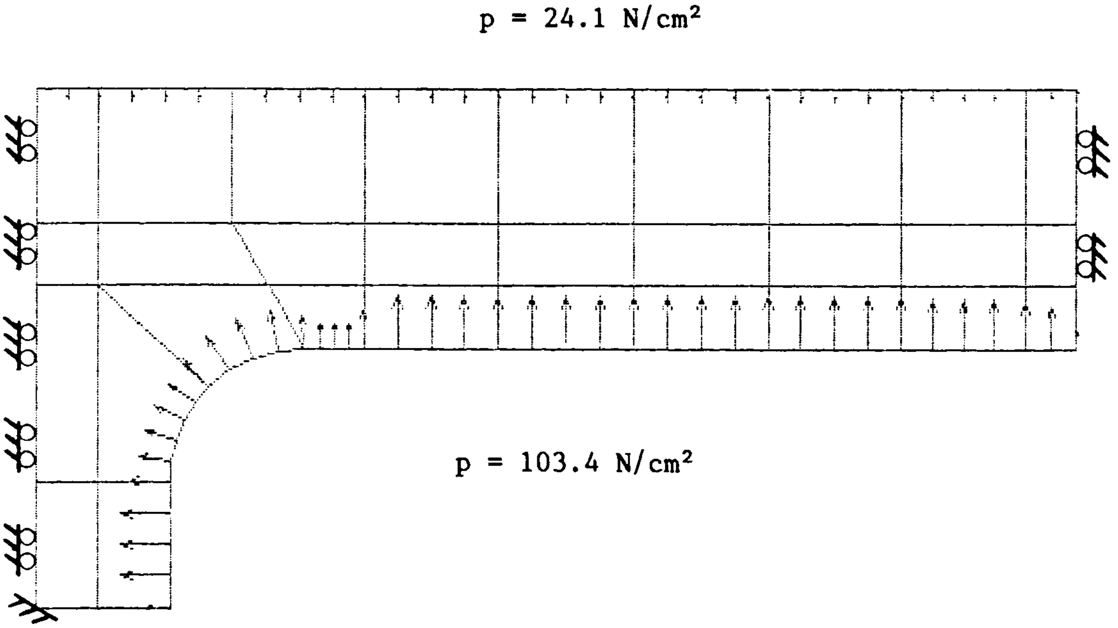

Figure 37. Ring #31, Pressure Loads and Constraints (Oil)

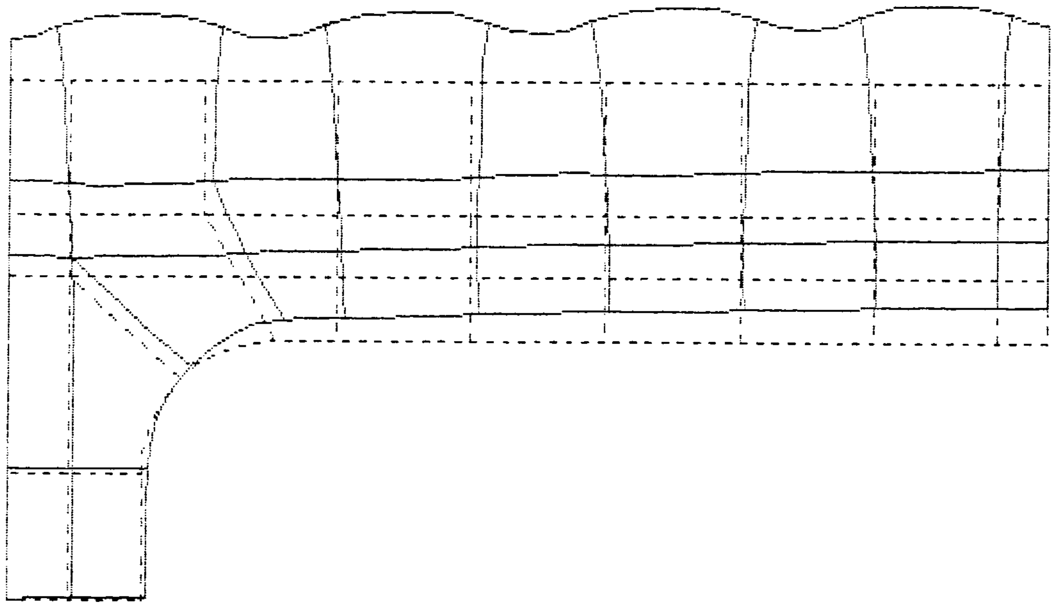

——— - Deflected Geometry

_ _ _ _ - Undeflected Geometry

Figure 38. Ring #31, Deflections (Oil)

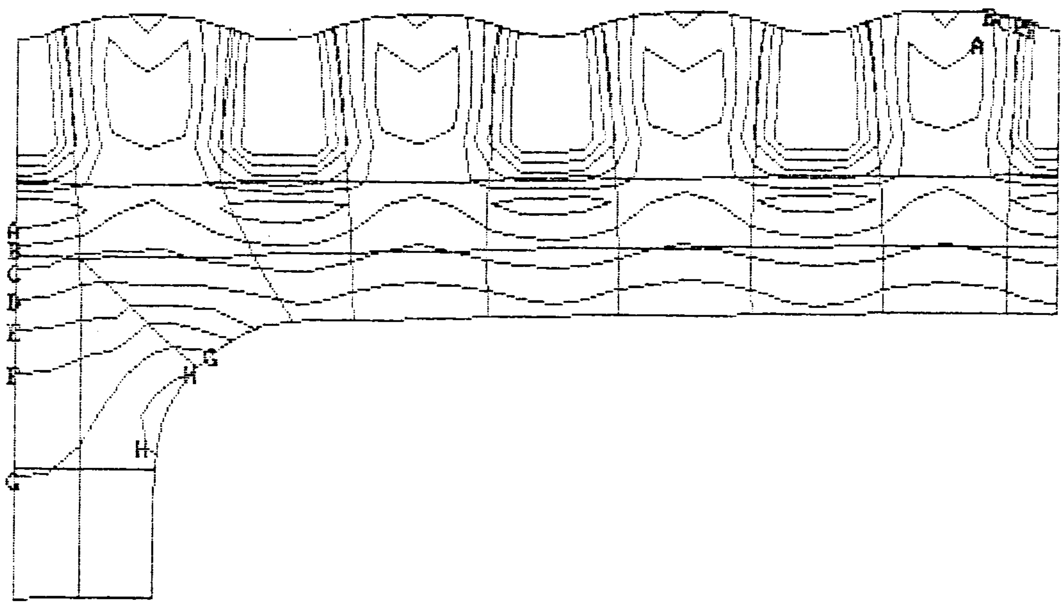

Maximum Principal
Stresses (N/cm^2)

A	-6.0E+04
B	-5.0E+04
C	-4.0E+04
D	-3.0E+04
E	-2.0E+04
F	-1.0E+04
G	1.0E-05
H	1.0E+04

Figure 39. Ring #31, Maximum Principal Stresses (Oil)

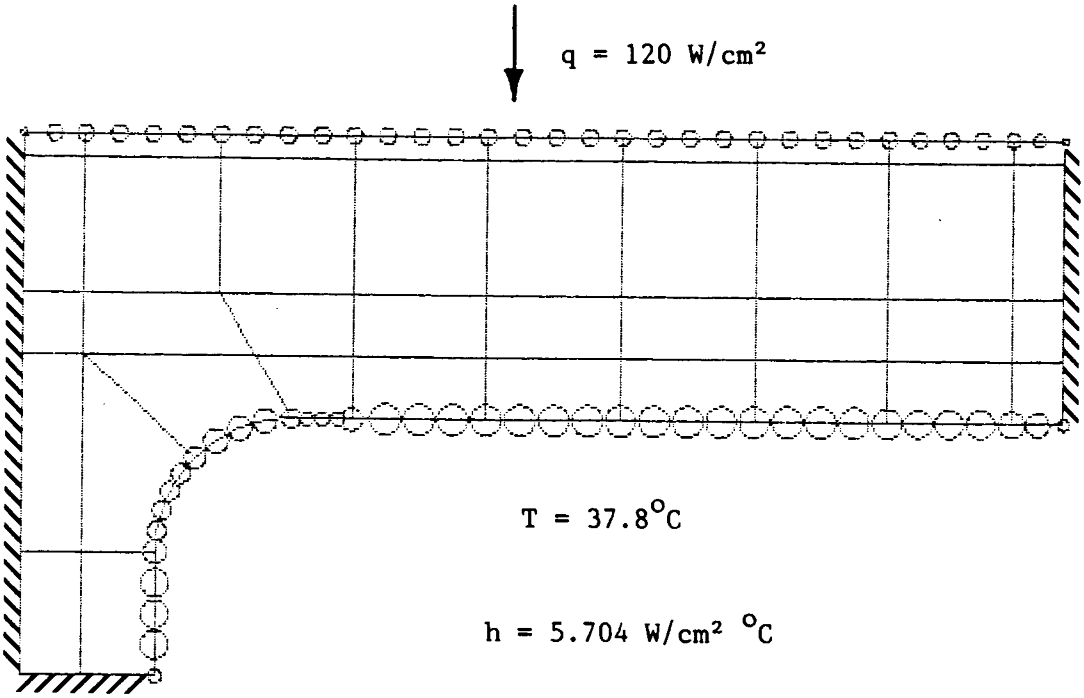

Figure 40. Ring #31, Thermal Boundary Conditions (Coal)

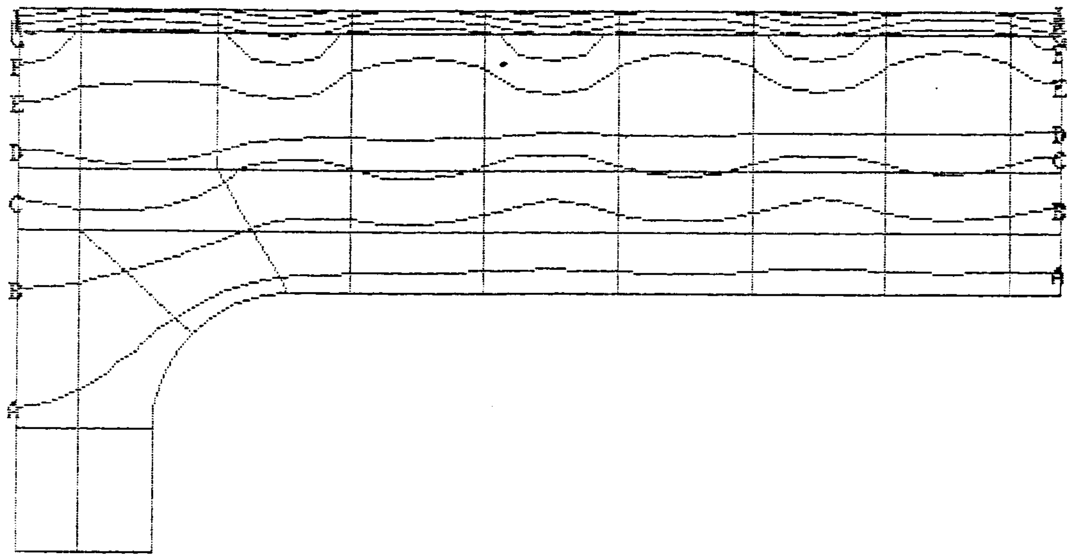

<u>Temperatures (°C)</u>

A	100.0
B	200.0
C	300.0
D	400.0
E	600.0
F	800.0
G	1000.0
H	1200.0
I	1400.0

Figure 41. Ring #31, Isotherms (Coal)

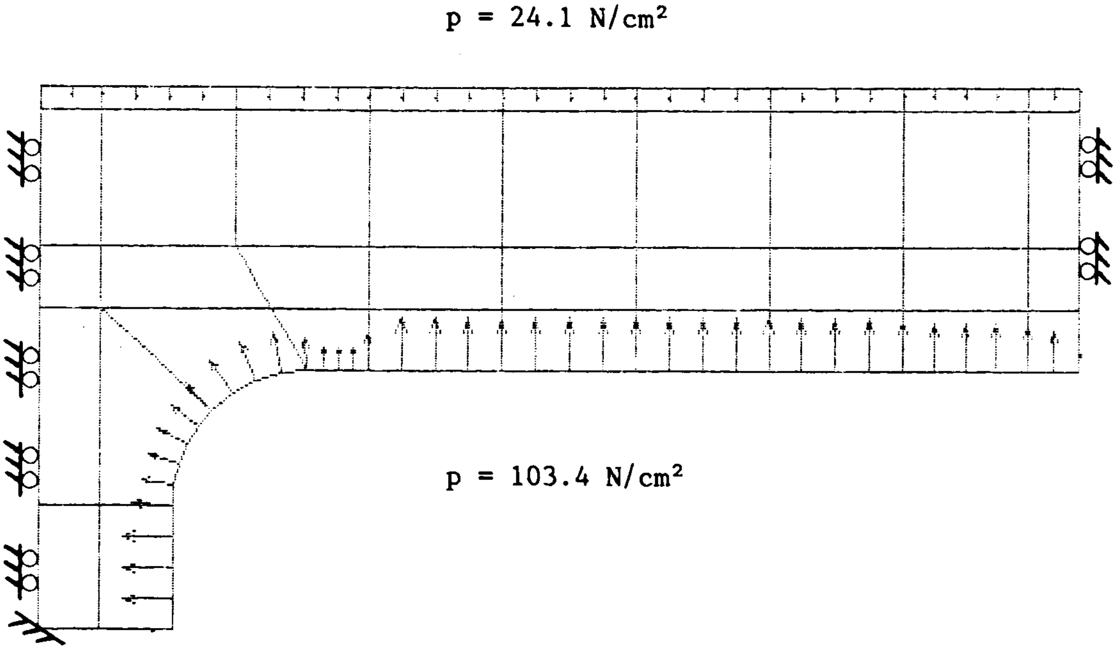

Figure 42. Ring #31, Pressure Loads and Constraints (Coal)

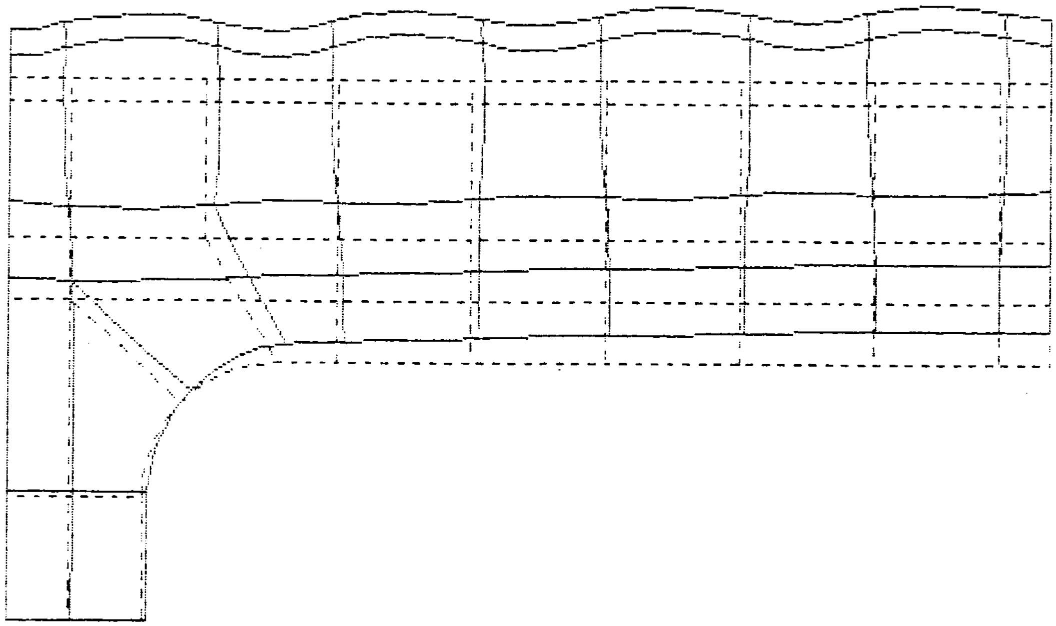

______ - Deflected Geometry

_ _ _ _ - Undeflected Geometry

Figure 43. Ring #31, Deflections (Coal)

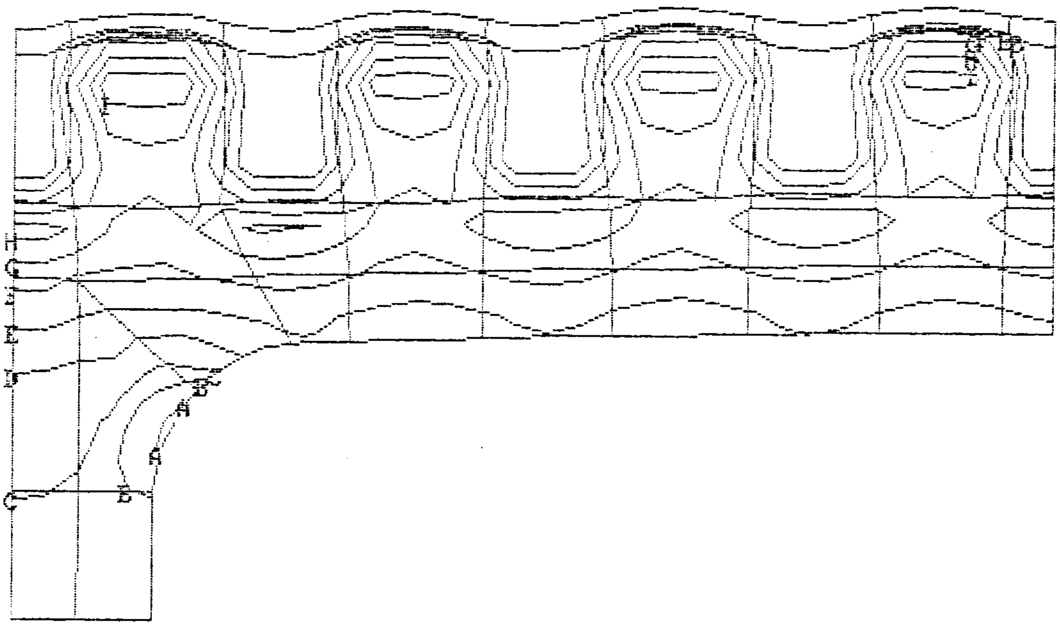

Maximum Principal
Stresses (N/cm^2)

A	2.0E+04
B	1.0E+04
C	1.0E-04
D	-2.0E+04
E	-4.0E+04
F	-6.0E+04
G	-8.0E+04
H	-1.0E+05
I	-1.2E+05
J	-1.4E+05

Figure 44. Ring #31, Maximum Principal Stresses (Coal)

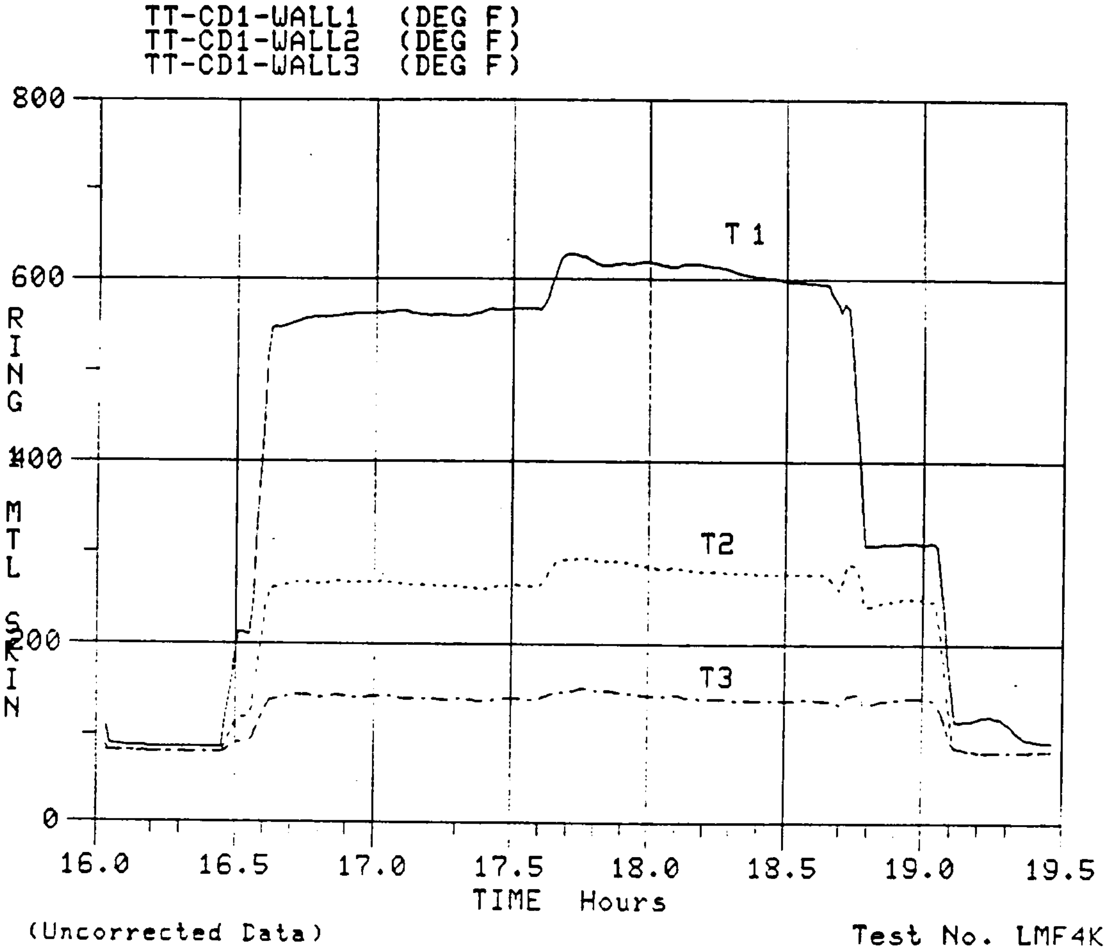

Figure 45. Thermocouple Measurements During Test LMF4K

VITA

Mary B. Groff, formerly Mary B. Biskner, was born in Detroit, Michigan on February 26, 1954. Two years later, she moved with her family to Stow, Ohio. In June 1972, she graduated from Our Lady of the Elms High School in Akron, Ohio. The following five years of study were spent at The University of Akron, receiving a B.S. in Civil Engineering in 1977. She accepted a graduate research assistantship in the fall of 1986 at The University of Tennessee Space Institute. She has worked, since then, in the Energy Conversion Programs at the Institute while studying for a Master of Science Degree in Mechanical Engineering.

She is married to Russell D. Groff and has three children. They presently reside in Winchester, Tennessee.